Electronic Supplementary Material (ESI) for Green Chemistry.

Supporting Information

Efficient reductive amination of HMF with well dispersed Pd nanoparticles immobilized in a porous MOF/polymer composite

Vikram V. Karve[a], Daniel T. Sun[a], Olga Trukhina[a], Shuliang Yang[a], Emad Oveisi[a,b], Jeremy Luterbacher[a], Wendy L. Queen[a,]*

* Corresponding author.

E-mail addresss : wendy.queen@epfl.ch (W. L. Queen)

a *Institute of Chemical Sciences and Engineering (ISIC), École Polytechnique Fédérale de Lausanne (EPFL), CH-1051 Sion, Switzerland*

b *Interdisciplinary Center for Electron Microscopy, École Polytechnique Fédérale de Lausanne (EPFL), CH-1015 Lausanne, Switzerland*

Nitrogen adsorption at 77 K and pore-size distribution using the carbon slit model

Pore-size distribution data is calculated using N_2 adsorption data at 77 K employing cylindrical geometry and the carbon slit as the model for calculation. The absence of the larger octahedral pore (around 2.1 nm) can be a qualitative indicator of the filling up of the pore with oligomeric and nanoparticulate species.

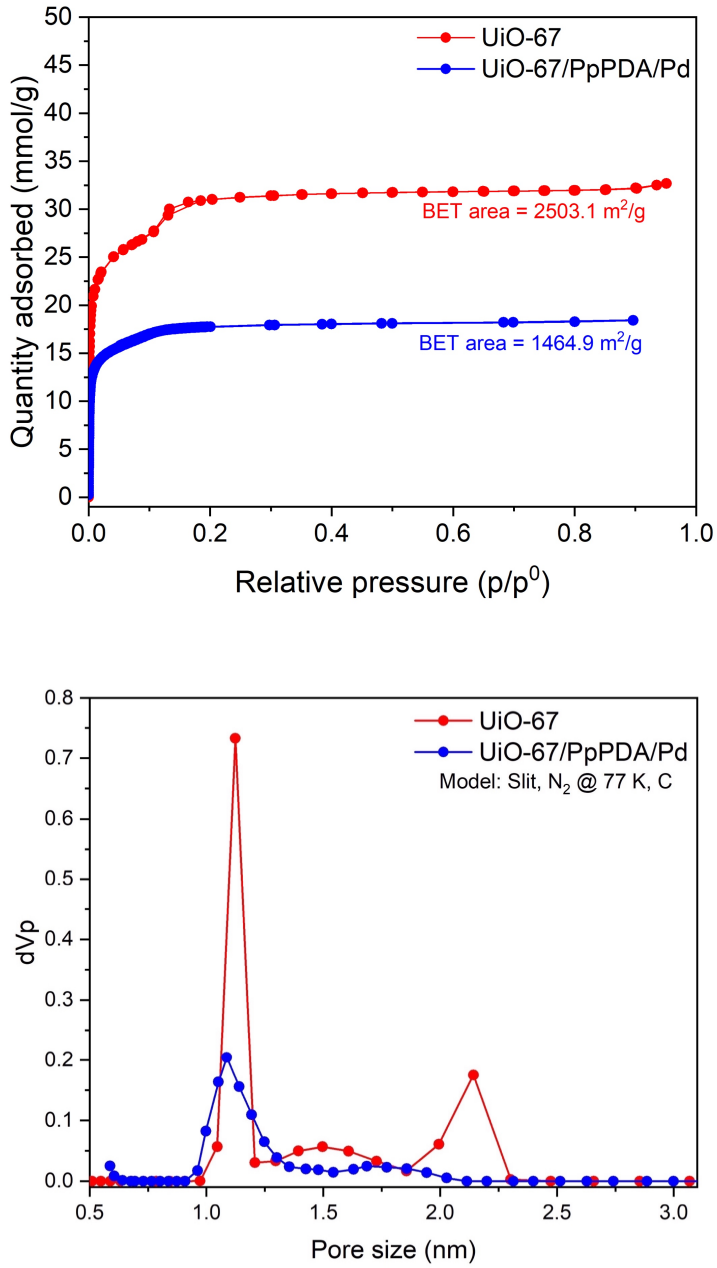

Figure S1 Nitrogen adsorption at 77 K and the corresponding pore size distribution plots for UiO-67 and the composite UiO-67/PpPDA/Pd catalyst

Elemental analysis of the as-synthesized catalysts

Table T1 Elemental analysis of the developed catalysts using a combination of ICP-OES, TGA and combustion analysis

Element	UiO-67		UiO-67/PpPDA/Pd (10 wt% polymer loading)		UiO-67/PpPDA/Pd (20 wt% polymer loading)		UiO-67/PpPDA/Pd (30 wt% polymer loading)	
	Found	Calc.	Found	Calc.	Found	Calc.	Found	Calc.
% Zr	26.5	26.7	25.9	26.7	26.3	26.7	26.9	26.7
% C	44.9	44.5	46.1	44.5	48.5	44.5	50.6	44.5
% N	1.3	1.4	3.2	1.4	4.3	1.4	5.9	1.4
% H	2.5	2.9	3.1	2.9	3.4	2.9	4.0	2.9
% Pd	0.41	0.5	0.45	0.5	0.42	0.5	0.44	0.5

Elemental analysis carried out for C, H, N elemental analysis under air

Zr and Pd content calculated independently from TGA and ICP-OES analysis

Calculated for $[Zr_6(\mu_3\text{-}O)_4(\mu_3\text{-}OH)_4(OH)_4(C_{14}H_8O_4)_5]DMF_2Cl_{0.5}$

MALDI-TOF mass spectroscopy for UiO-67/PpPDA/Pd

The MALDI-TOF-MS data for the UiO-67/PpPDA/Pd composite indicates presence of polymeric species comprising of 3, 4, 6 and, 8 units of the monomer. The corresponding m/z peaks are 341, 453, 698 and 805 respectively.

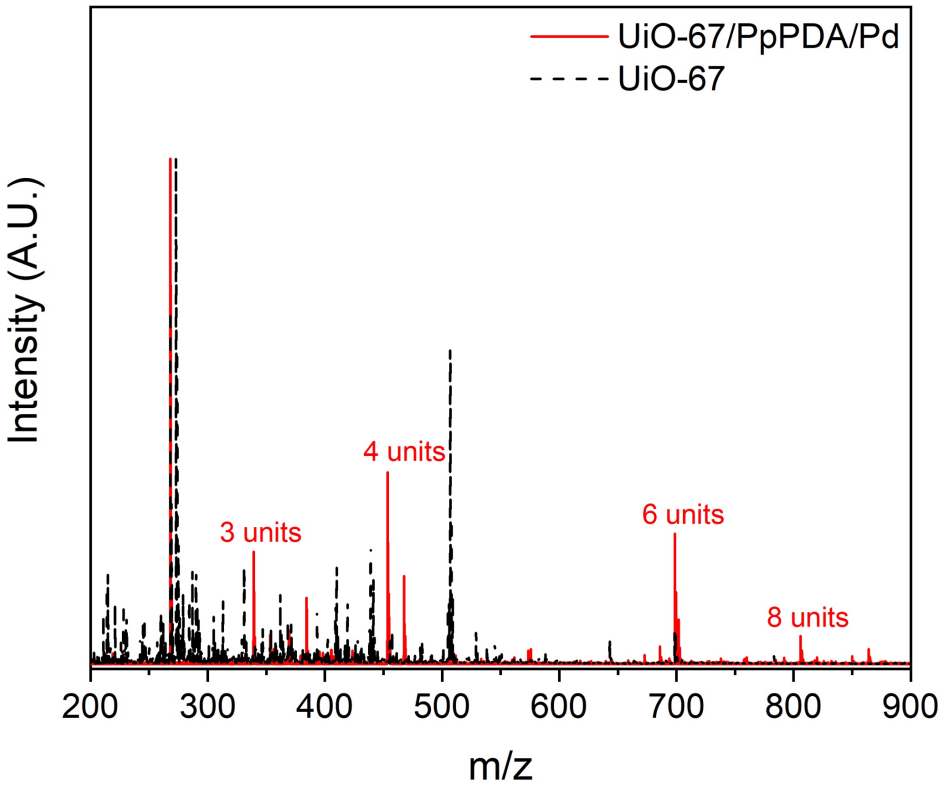

Figure S2 MALDI-TOF-MS data for UiO-67/PpPDA/Pd

MALDI-TOF mass spectroscopy for PpPDA/Pd

The MALDI-TOF-MS data for the PpPDA/Pd composite indicates presence of polymeric species comprising of 7, 8, 9 and 11 units of the monomer. The corresponding m/z peaks are 719, 805, 950 and 1105 respectively.

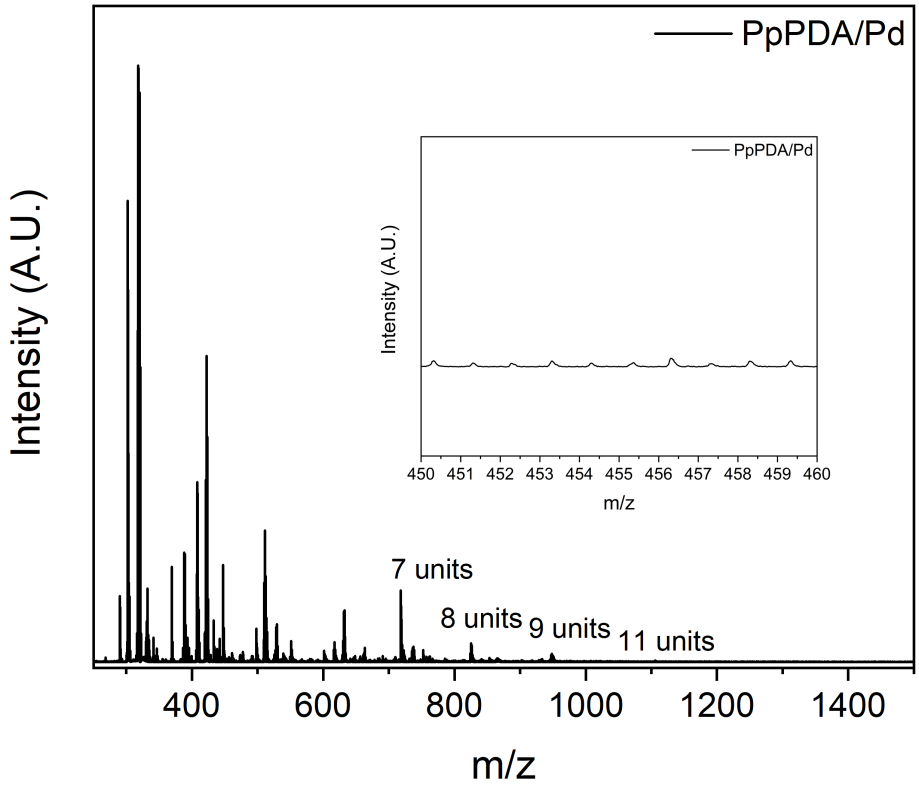

Figure S3 MALDI-TOF-MS data for PpPDA/Pd indicating absence of lower molecular weight oligomeric units; (Inset) A closer look at the range between 450-460 m/z indicating absence of peaks corresponding to the 4 unit oligomer (m/z = 453)

Attenuated total reflectance infrared spectroscopy (ATR-IR)

Attenuated total reflectance infrared (ATR-IR) spectra of the bare framework and the composite was collected on a Perkin-Elmer Frontier MIR/FIR equipped with a Quest ATR attachment. The sample was pressed on a diamond window with a recording window between 4000 and 400 cm^{-1} at a resolution of 4 cm^{-1}. The new peak which emerges in the composite at 732 cm^{-1} indicates presence of the secondary C-N-C stretch which is representative of the polymer[1],[2]

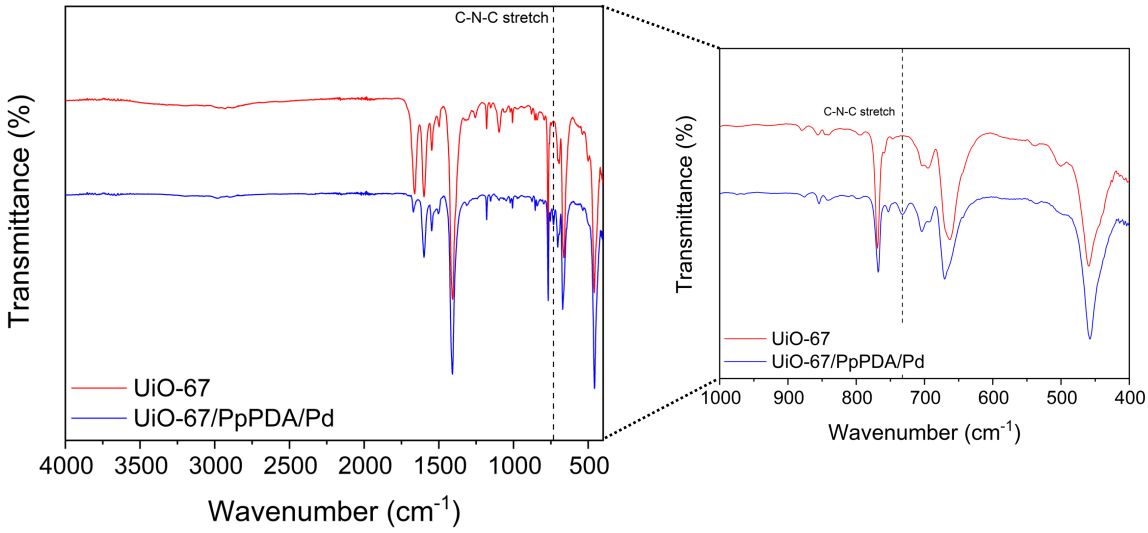

Figure S4 ATR-IR spectrum of UiO-67 and UiO-67/PpPDA/Pd

Scanning electron microscopy (SEM):

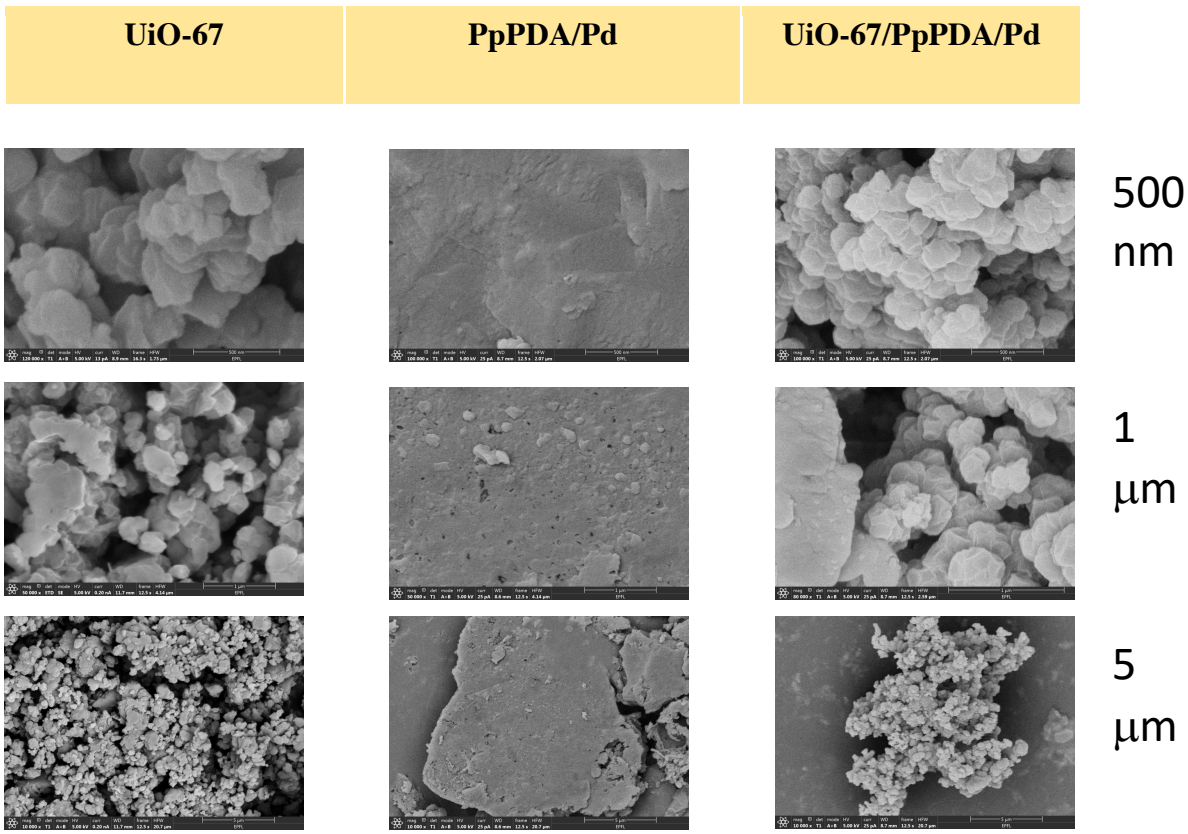

Figure S5 Scanning electron microscopy (SEM) images for the bare framework (UiO-67), the polymer-Pd composite (PpPDA/Pd) and the MOF composite (UiO-67/PpPDA/Pd). The numbers on the right represent the size of the scale bars.

TEM imaging and catalytic activity of UiO-67/PpPDA/Pd catalyst

Characterization of the pristine UiO-67/PpPDA/Pd composite catalyst by TEM imaging.

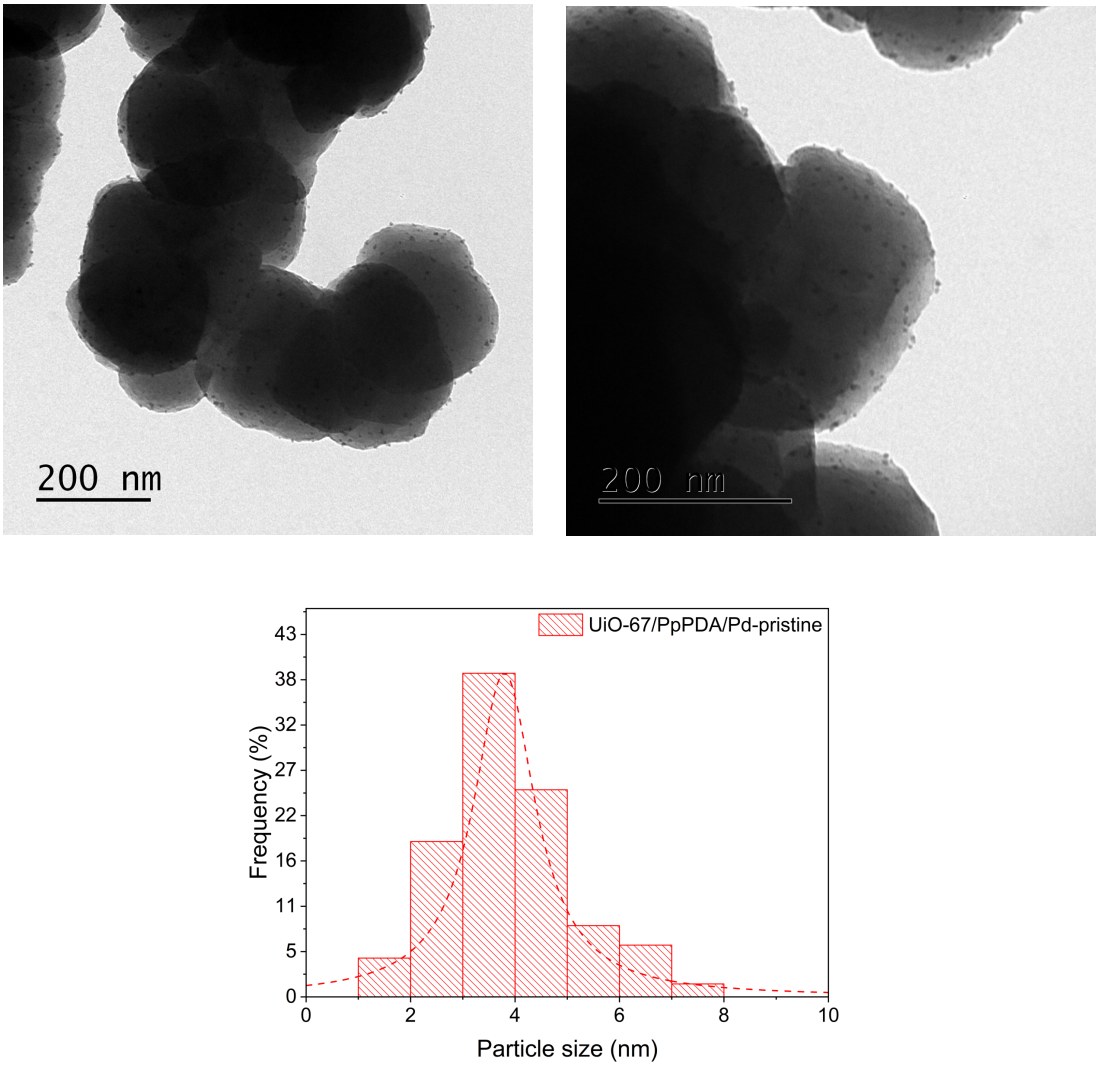

Figure S6 TEM images and the corresponding particle size distribution for the pristine UiO-67/PpPDA/Pd catalyst

Titrimetric evaluation of the presence of defects in the composite

The titrimetric study, the assignment of all the peaks, and the calculation of the number of defects from the derivative spectrum was carried out based on the work previously reported.[18] The Zr-OH_2 and Zr-OH represent typical defect sites present in the UiO series of frameworks.

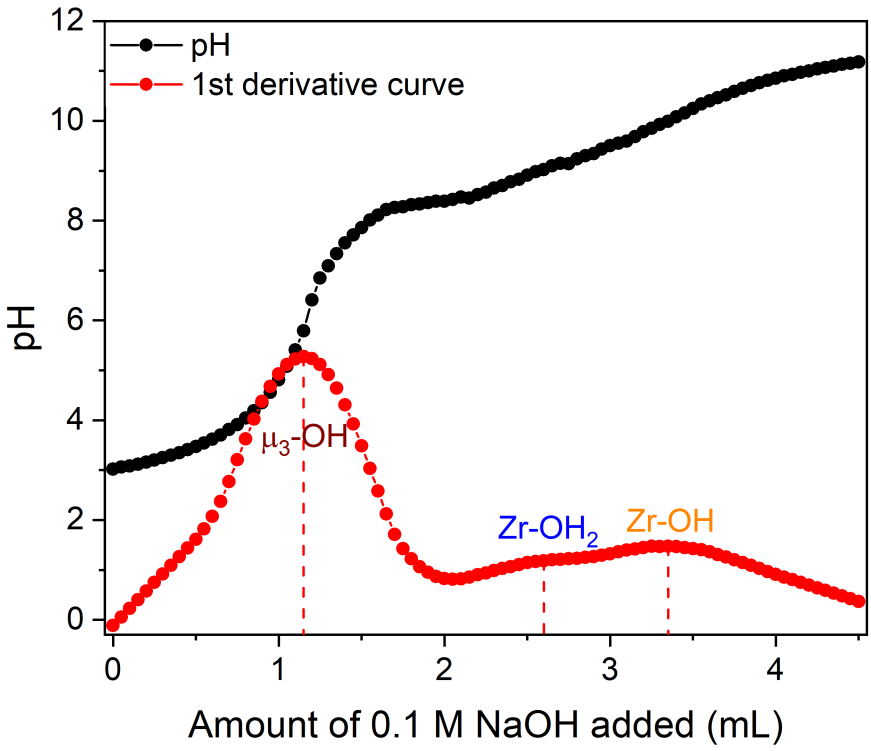

Figure S7 Titrimetric study for the UiO-67/PpPDA/Pd composite

BF-EDX imaging and spectroscopy of UiO-67/PpPDA/Pd

EDX analysis on the microtomically sliced UiO-67/PpPDA/Pd composite. The two regions show the EDX spectra for the resin material (green) in which the composite is embedded and the composite itself (orange). The scale bar in the BF image corresponds to a length of 200 nm.

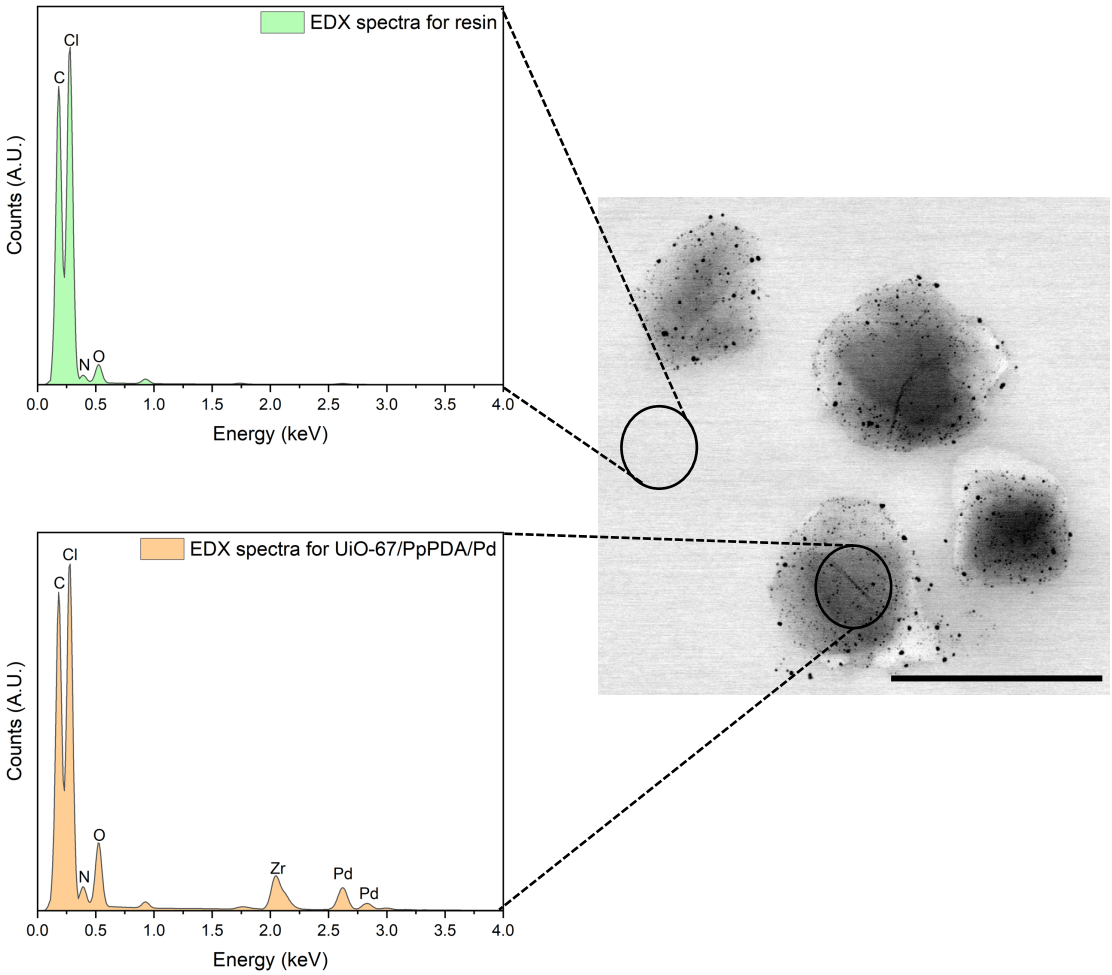

Figure S8 Bright-field EDX spectra for the UiO-67/PpPDA/Pd composite inside and outside the MOF crystal

TEM images of polymer-Pd composite

Transmission electron microscopy images for the polymer-Pd composite indicating, the morphology of the polymer and the lack of distinct Pd nanoparticles indicating that part of the Pd is unreduced. The reduced Pd particles have a size between 20-35 nm in terms of their size with the average size being around 25 nm. The particle size analysis was carried out using the ImageJ software.

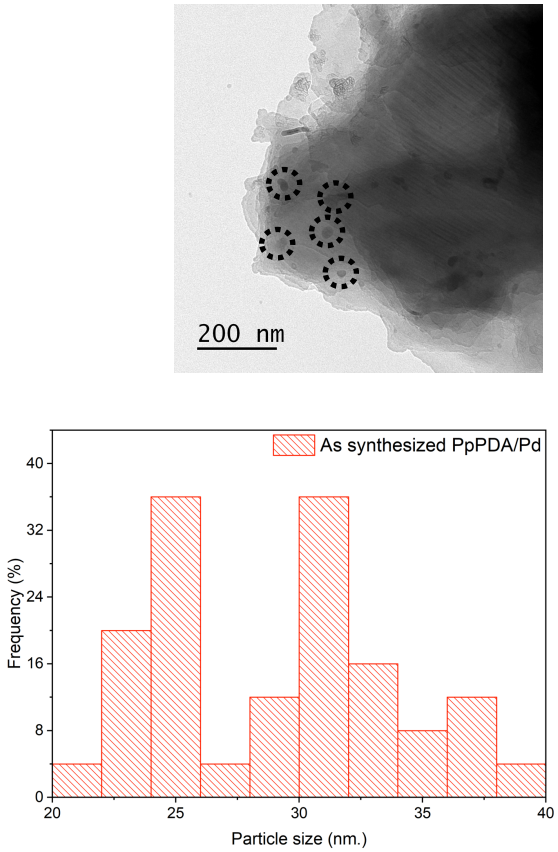

Figure S9 TEM images and the corresponding particle size distribution of the PpPDA/Pd composite

Hot filtration study

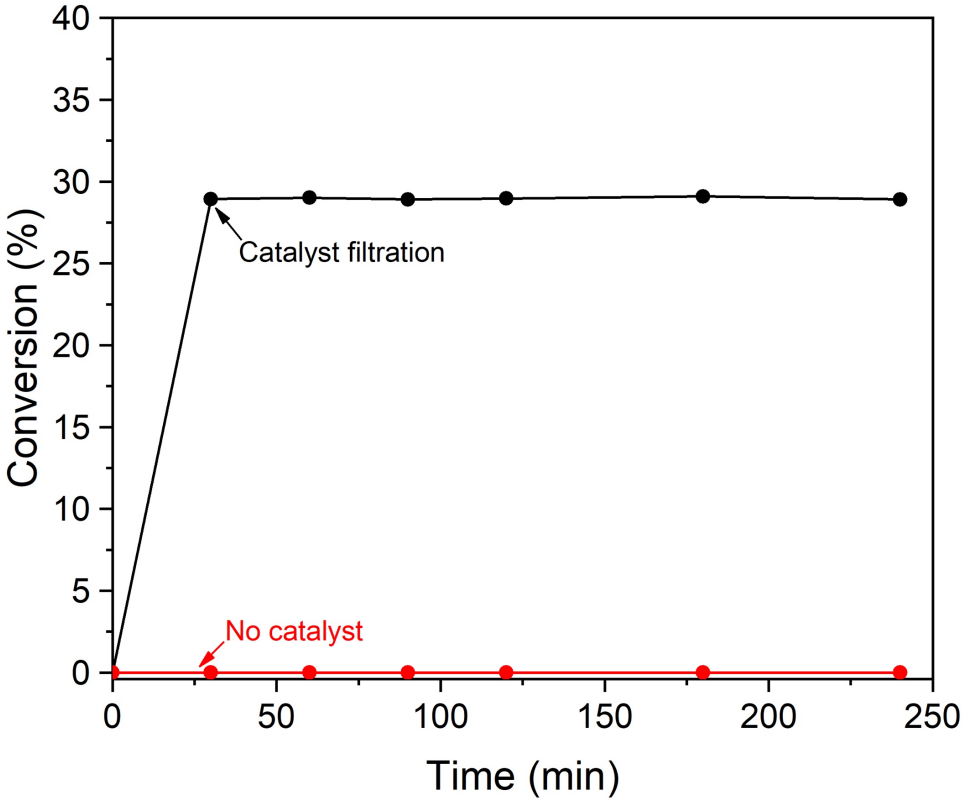

Figure S10 Hot filtration studies indicating that no conversion of HMF occurs after filtration of the catalyst; thereby implying heterogeneity of the catalytic process

TEM imaging and the corresponding particle size distributions before and after cycling of as prepared Fe-BTC/Pd

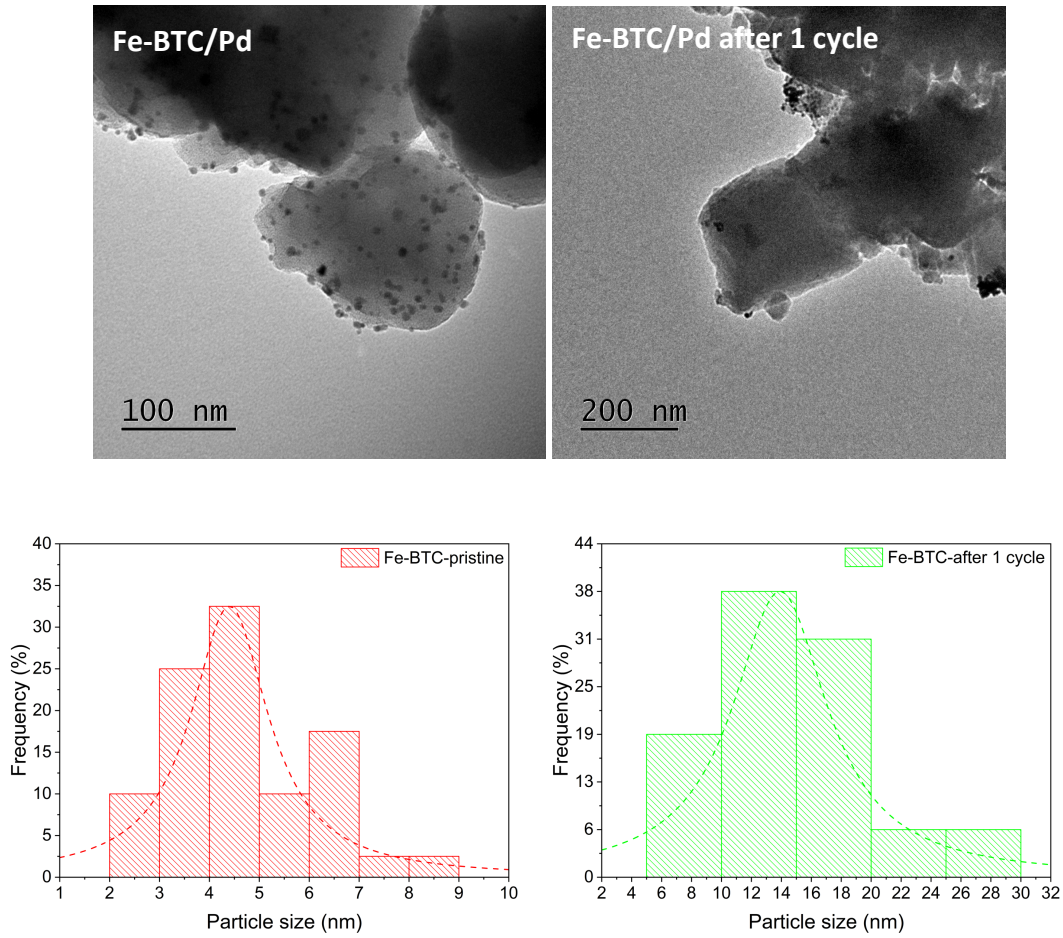

Figure S11 TEM images and the corresponding particle size distributions (determined using ImageJ) for Fe-BTC/Pd

TEM imaging and the corresponding particle size distributions before and after cycling of as prepared UiO-67/Pd and as purchased Pd/C

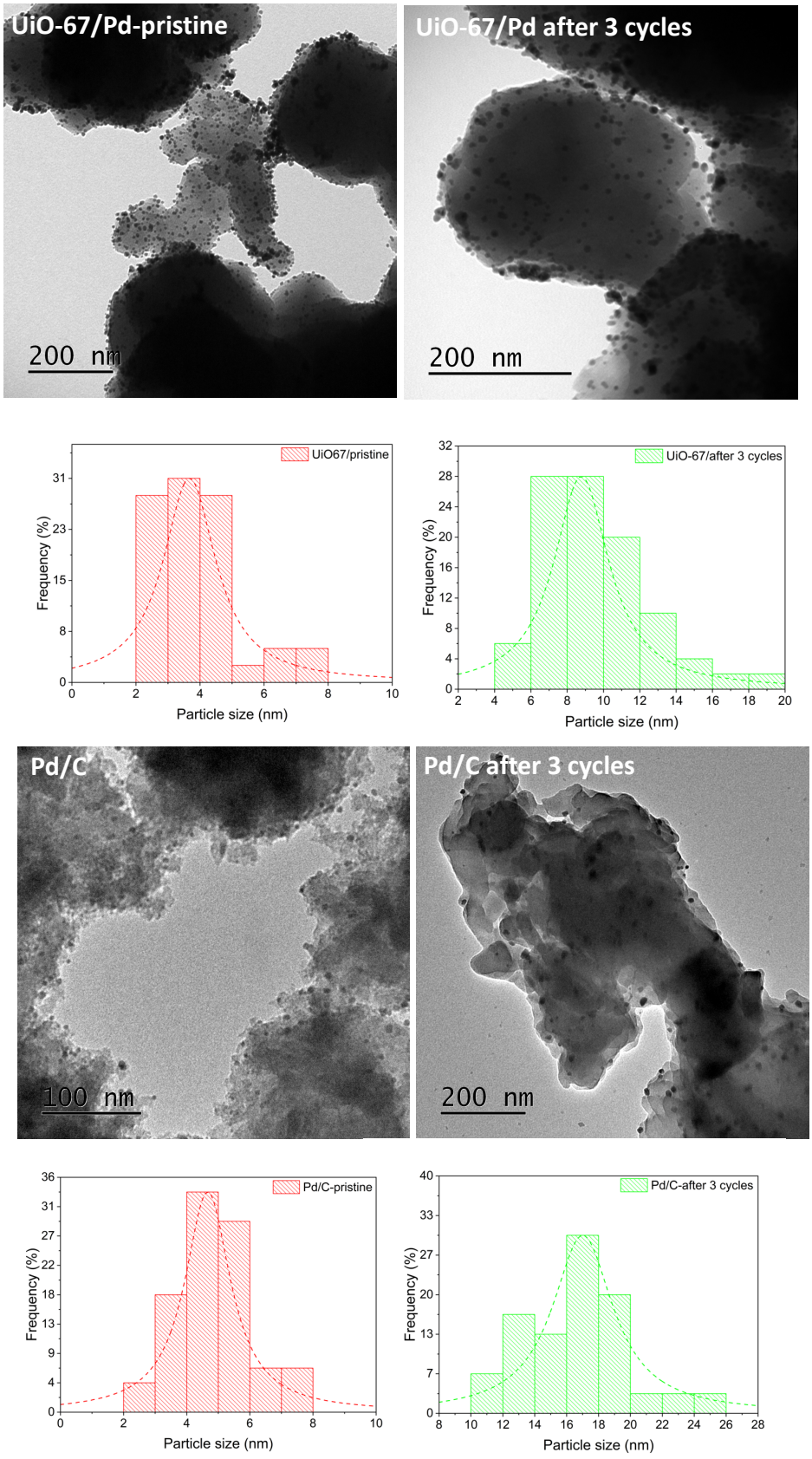

Figure S12 TEM images and the corresponding particle size distributions (determined using ImageJ) for UiO-67/Pd and Pd/C before and after cycling

Powder XRD of the UiO-67/Pd and Fe-BTC/Pd catalysts

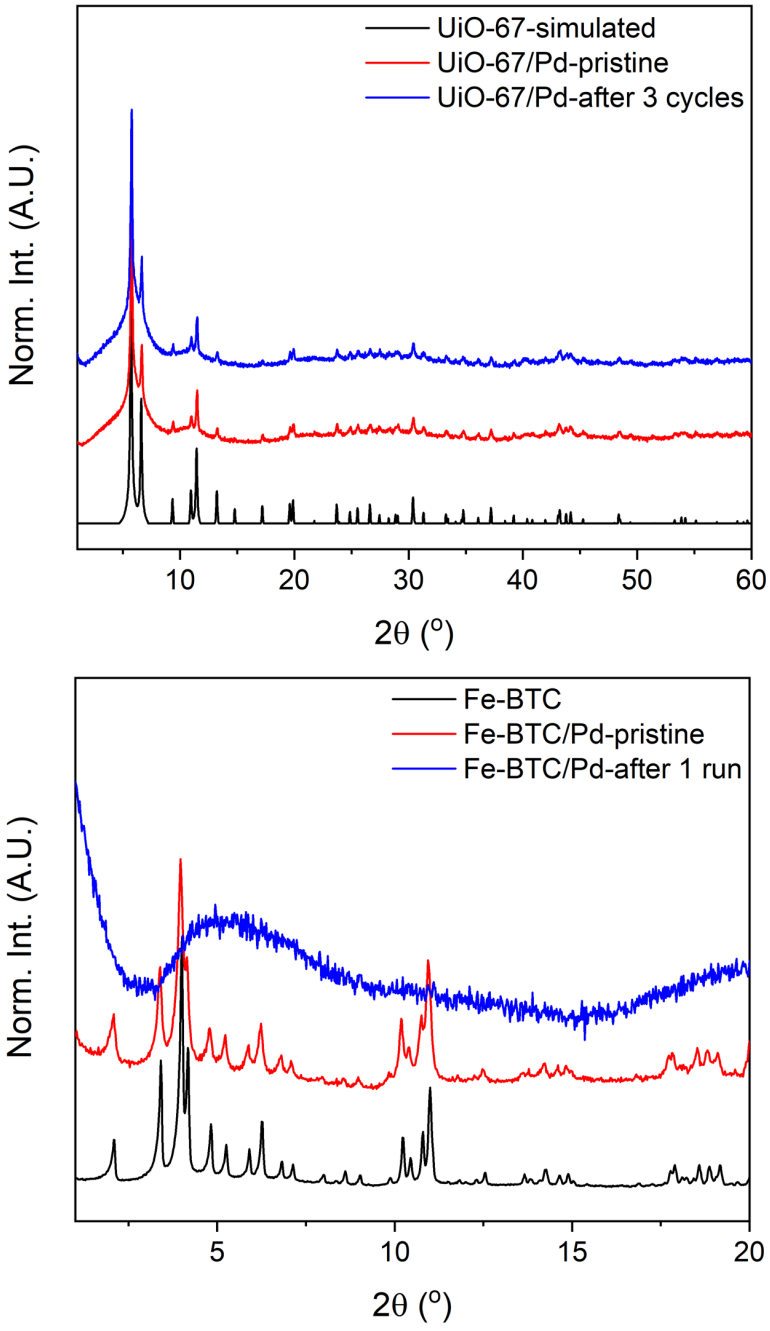

Figure S13 Powder X-ray diffractograms for UiO-67/Pd and Fe-BTC/Pd catalysts before and after cycling indicating the stability of the UiO structure to cycles and the instability of the Fe-BTC structure respectively during the cycling process

TEM imaging and the corresponding particle size distribution for UiO-67/PpPDA/Pd catalyst after 10 cycles

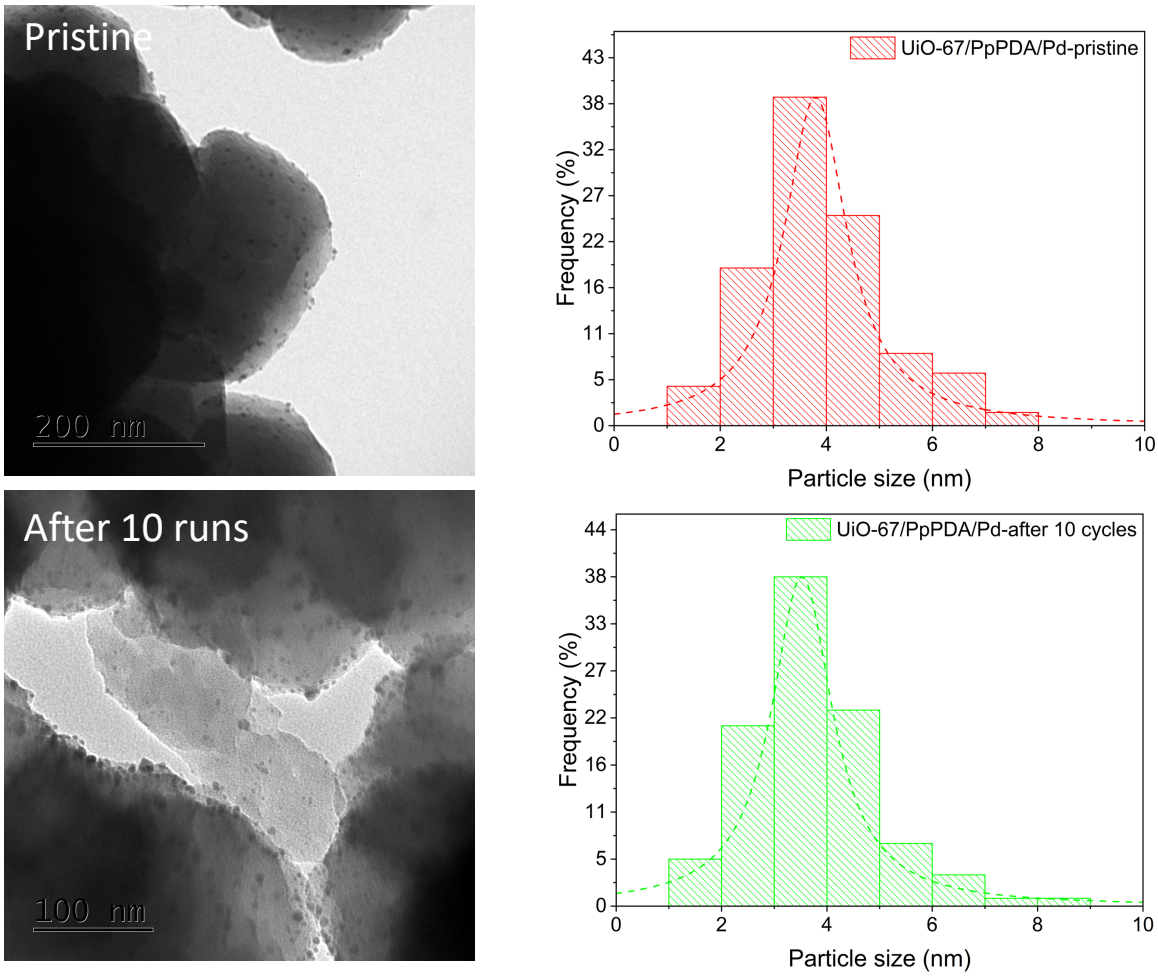

Figure S14 TEM images and the corresponding particle size distributions (determined using ImageJ) for UiO-67/PpPDA/Pd before and after 10 cycles

TEM imaging and the corresponding particle size distribution for UiO-67/PpPDA/Pd catalyst after 15 cycles

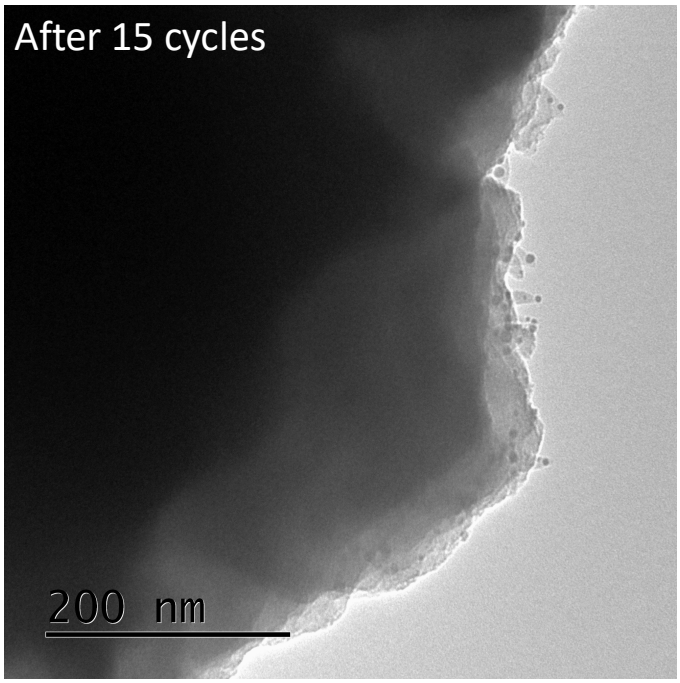

Figure S15 TEM images and the corresponding particle size distributions (determined using ImageJ) for UiO-67/PpPDA/Pd after 15 cycles

Table T2 ICP-OES measurements of the amount of Pd in the pristine catalyst, in the catalyst after 15 cycles and in the reaction mixture after 15 cycles

Sample	**Pd (wt%) in pristine catalyst**	**Pd (wt%) after 15 cycles**	**Pd (ppm) in reaction mixture after 15 cycles**
UiO-67/PpPDA/Pd	0.40(2)	below detection limit	4.0(3)
All values were determined by ICP-OES analyses, triplicating each experiment for consistency			

MALDI-MS-TOF and ICP-OES analyses for UiO-67/Pd, Fe-BTC/Pd, UiO-67/PpPDA/Pd and Pd/C catalysts to check for leaching of Pd and polymeric units

Table T3 ICP-OES measurements of the amount of Pd in the catalyst after soaking under the reaction conditions

Sample	Pd (wt%) in pristine catalyst	Pd (wt%) after 2 hour soaking	Pd (wt%) after 6 hour soaking	Pd (wt%) after 24 hour soaking
UiO-67/Pd	0.40(6)	0.38(1)	0.14(7)	below detection limit
Fe-BTC/Pd	0.47(2)	0.11(5)	below detection limit	below detection limit
Pd/C	1.00(5)	0.98(4)	0.24(1)	below detection limit
UiO-67/PpPDA/Pd	0.40(2)	0.38(1)	0.38(1)	0.34(2)
All values were determined by ICP-OES analyses, triplicating each experiment for consistency				

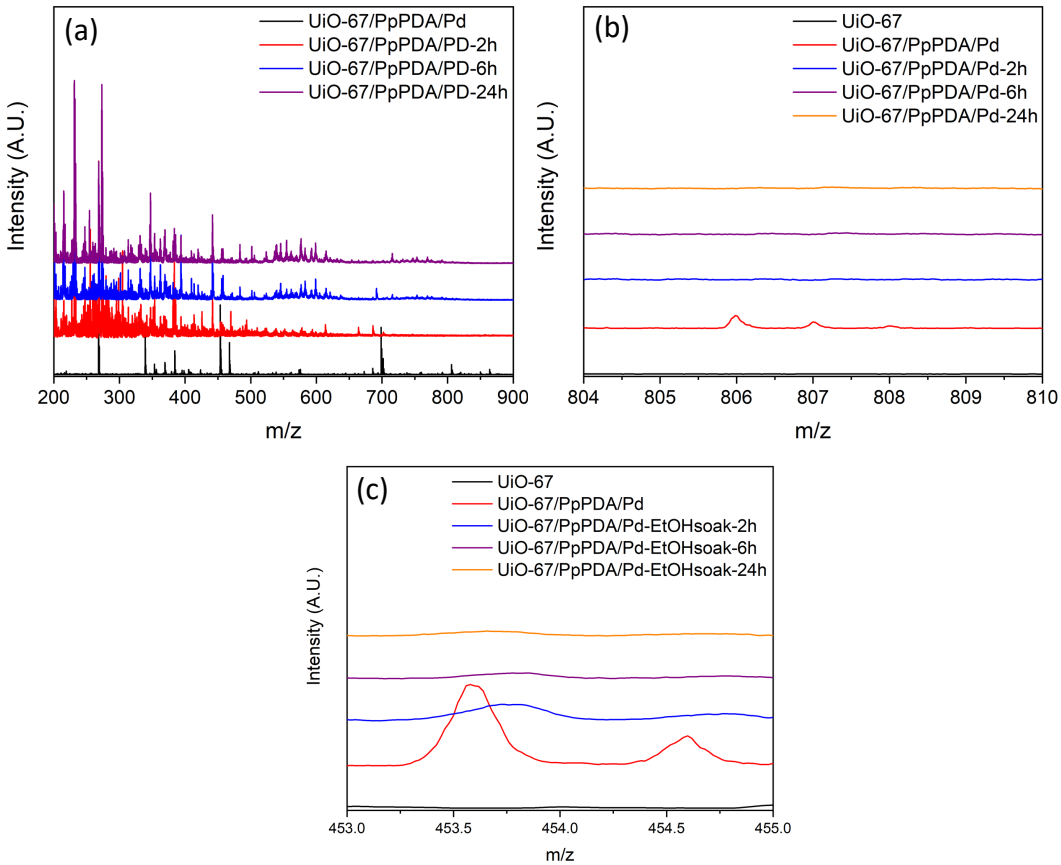

Figure S16 MALDI-TOF-MS data for the UiO-67/PpPDA/Pd catalyst showing no leaching of polymer up to 24 hours. We show specifically two zoomed in regions from 804-810 and from 453-455 which correspond to the 4 and 8 units of the monomer making the polymeric species. Further, the spectrum in red in figures (a), (b), and (c) corresponds to the pristine catalyst, UiO-67/PpPDA/Pd, which was digested.

Turnover number (TON) and turnover frequency (TOF) calculations

The turnover numbers and turnover frequencies are calculated at a conversion level of 40%. The turnover number and turnover frequencies were initially defined according to Kozuch et. al.[1] However, this definition cannot be applied in our case because of the multi-step nature of the reaction, hence, the kinetic order of the reaction is not necessarily an integer.

$$Turnover\ number\ (TON) = \frac{Moles\ of\ product}{Moles\ of\ catalytically\ active\ species\ used}$$

$$Turnover\ frequency\ (TOF) = \frac{TON}{Time\ of\ reaction\ (in\ hours)}$$

Table T4 Turnover number and frequency calculations for various catalysts reported for reductive aminations in literature

Comparison for (5-((phenylamino)methyl)furan-2-yl)methanol						
S.No.	Reference	Catalyst	Reaction conditions	Turnover number	Turnover frequency (h^{-1})	Recycles
1	2	Au/TiO_2 with CO atm	20 bar CO, 60°C, 2.5h	0.4	0.2	5
2	Catalyst developed in this paper	UiO-67/PpPDA/Pd	5 bar H_2, 50°C, 2h	604.8	302.4	15
Comparison for (5-(aminomethyl)furan-2-yl)methanol						
3	3	Co-DABCO-TPA@C-800	40 bar H_2, 120°C, 15h	0.05	0.003	6
4	4	Ru/Nb_2O_5	40 bar H_2, 1 bar NH_3, 100°C, 2h	10.52	2.63	--
5	5	Transaminase	30°C, 24h	--	--	Homog.
6	6	Rh/Al_2O_3	20 bar H_2, 80°C, 2h	6.52	3.26	5
7	Catalyst developed in this paper	UiO-67/PpPDA/Pd	5 bar H_2, 50°C, 2h	556.8	278.4	15
Comparison for *N*-(furan-2-ylmethyl)aniline						
8	7	Et_3SiH (3 eq), $BiCl_3$ (30mol%)	25°C, 23h	12.45	6.24	Homog.
9	8	Pd/NiO	1 bar H_2, 25°C, 12h	2	0.16	5
10	9	Pd/C	25°C, 0.5h	0.48	0.24	--
11	10	$ReOBr_2$/(Hhmpbta)PPh_3	70°C, 0.5h	0.16	0.32	--
12	11	$AlCl_3$/PHMS	70°C, 12h	0.2	0.016	3
13	12	PS-Pd-NHC	35 bar H_2, 80°C, 8h	16	2	6
14	13	$NaBH_4$	25°C, 0.1h	0.4	0.8	Homog.
15	14	PPh_3AuCl, AgOTf	25°C, 0.7h	0.4	0.6	Homog.
16	15	$CeCl_3.7H_2O$	25°C, 0.5h	12.12	6.06	Homog.
17	16	$FeCl_3$, PMHS	60°C, 24h	4.25	2.12	Homog.
18	17	$Zn(Otf)_2$, PMHS	60°C, 24h	6.38	3.19	Homog.
19	Catalyst developed in this paper	UiO-67/PpPDA/Pd	5 bar H_2, 50°C, 2h	595.2	297.6	15

Kinetic study of HMF conversion as a function of time

The recyclability of the composite catalyst is studied by probing the HMF conversion as a function of time for each recycling step. Each data point was gathered as a separate reaction and the same was triplicated to get a reasonable error estimate.

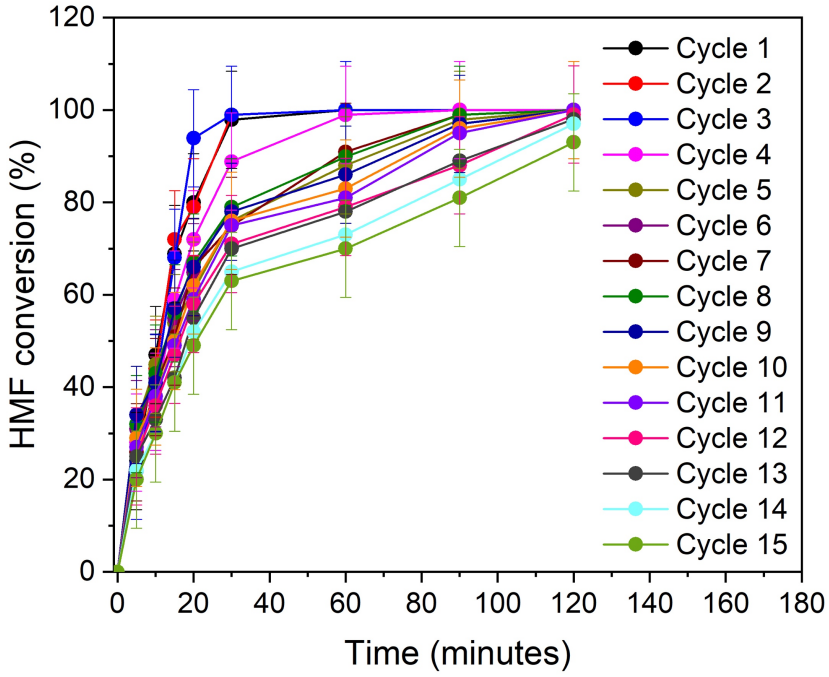

Figure S17 Kinetics of HMF conversion as a function of time for each recycling step

Powder X-ray diffraction data

XRD pattern of the catalyst after 16 runs showing loss of crystallinity of the MOF framework from repeated cycling.

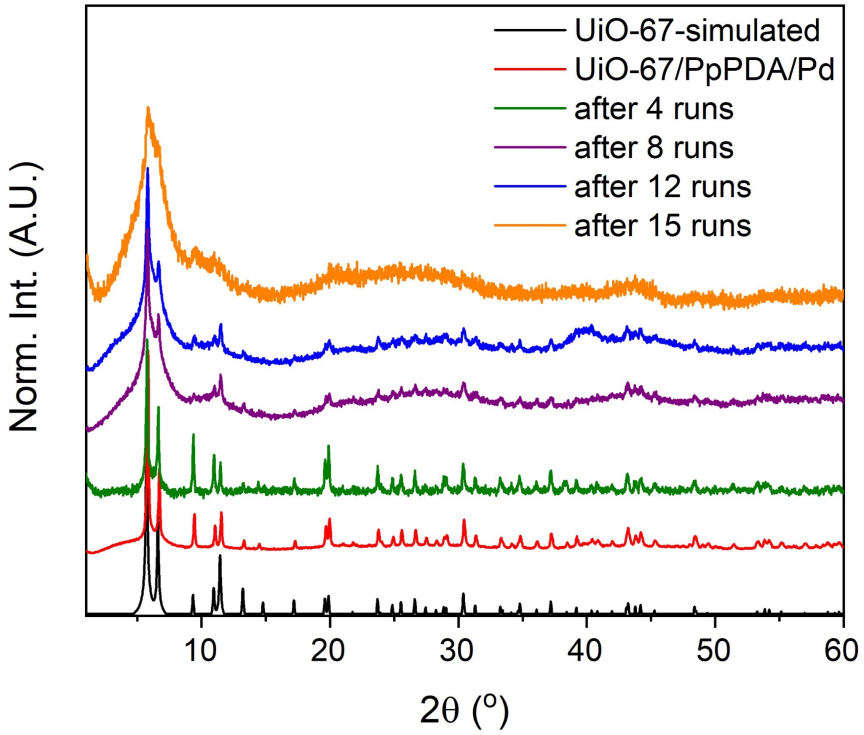

Figure S18 PXRD patterns of the pristine UiO-67/PpPDA/Pd catalyst and the catalyst after 4, 8, 12 and 15 cycles

Recycling data at 100% conversion of HMF

Cycling data for the reductive amination of HMF with aniline, at 100% conversion, and the selectivity towards the intermediate imine and the final amine product. All values were determined from ^{1}H NMR studies. The reaction conditions used were as follows: 0.24 mmol HMF; 0.24 mmol aniline; 5 mL ethanol; 10 mg UiO-67/PpPDA/Pd (0.4 wt% Pd); 5 bar H_2; 50°C; 2 hours.

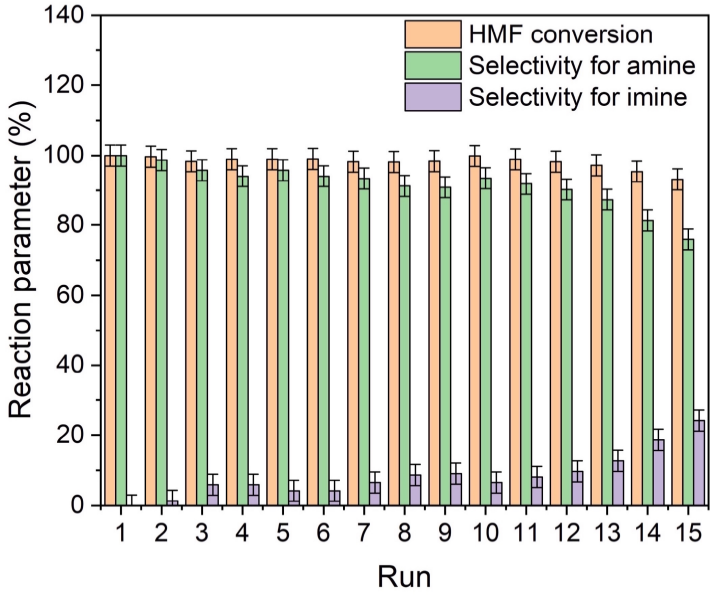

Figure S19 Cycling study for UiO-67/PpPDA/Pd at 100% conversion

Recycling data at 40% conversion of HMF

Cycling data for the reductive amination of HMF with aniline, at 40% conversion. All values were determined from ^{1}H NMR studies. The reaction conditions used were as follows: 0.24 mmol HMF; 0.24 mmol aniline; 5 mL ethanol; 10 mg UiO-67/PpPDA/Pd (0.4 wt% Pd); 5 bar H_2; 50°C; 15 minutes. The data suggests a steady decrease in the HMF conversion which co-relates with the slow degradation of the MOF support as evidenced by PXRD (Figure S8).

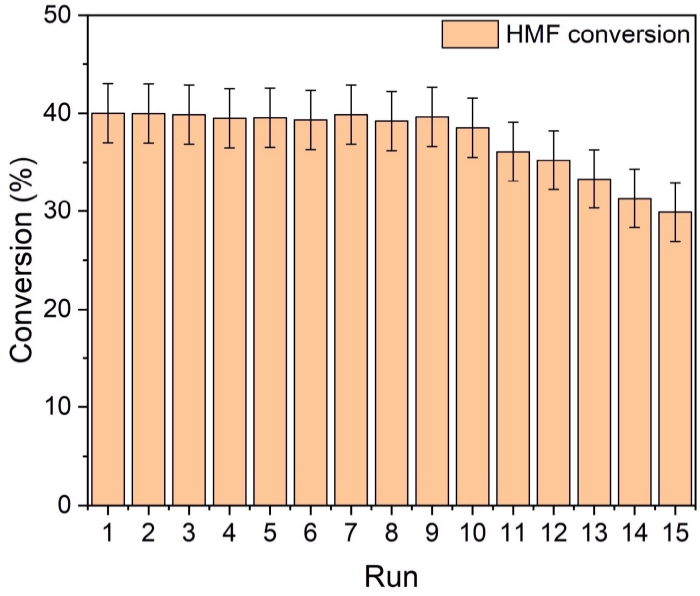

Figure S20 Cycling study for UiO-67/PpPDA/Pd at 40% conversion

Effect of the cycle number on the initial rate of HMF consumption for UiO-67/Pd and UiO-67/PpPDA/Pd

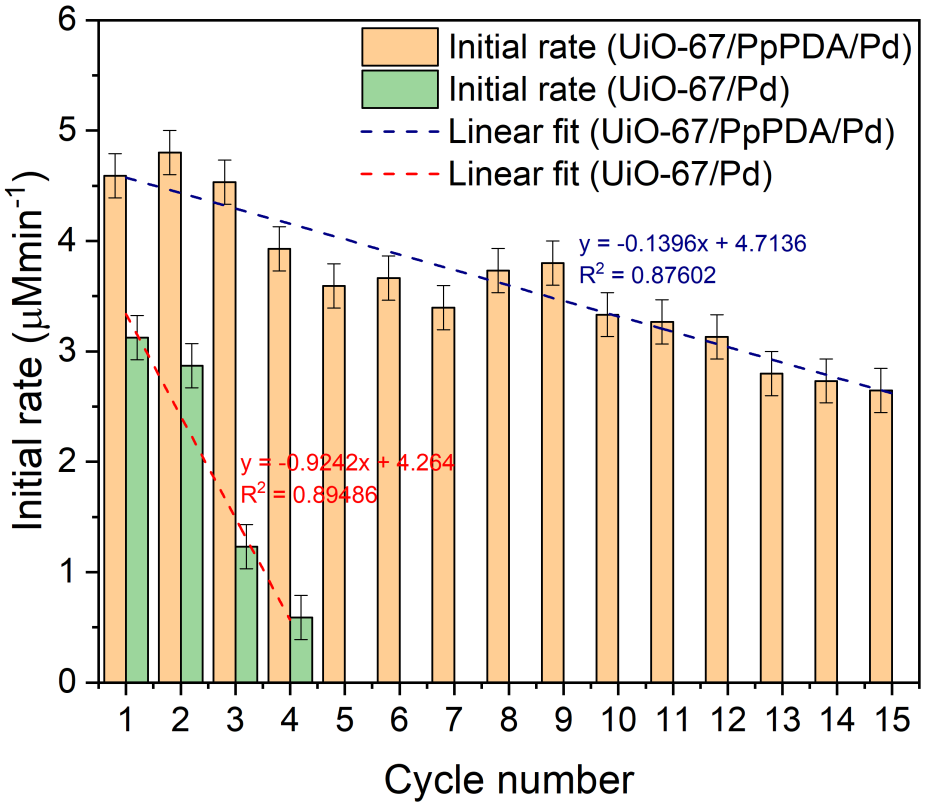

Figure S21 Effect of cycling on the initial rate of HMF consumption for UiO-67 and UiO-67/PpPDA/Pd indicating clearly the effect of the N-rich polymer in stabilizing the Pd nanoparticles and extending the recyclability

Powder XRD for UiO-67/PpPDA/M (M=Cu, Ni, Co) composites

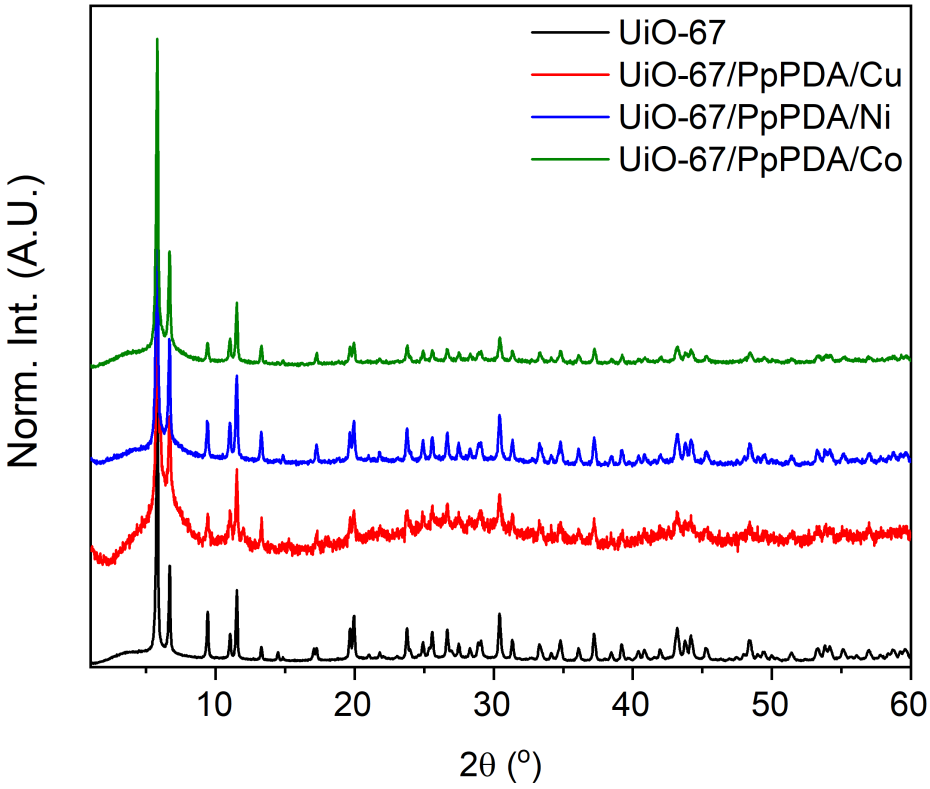

Figure S22 Powder XRD for the UiO-67/PpPDA/M (M=Cu, Ni and Co) composites

TEM images for UiO-67/PpPDA/M (M=Cu, Ni, Co)

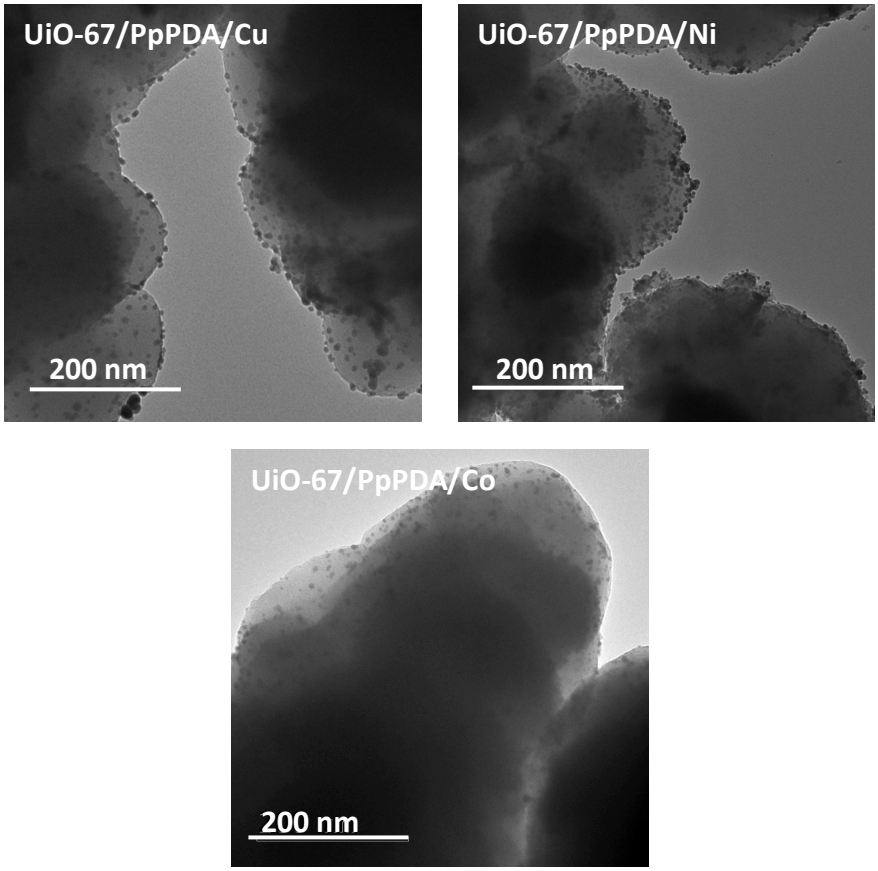

Figure S23 TEM imaging of the UiO-67/PpPDA/M (M=Cu, Ni and Co) composites

Nitrogen sorption isotherms at 77 K for UiO-67/PpPDA/M (M=Cu, Ni, Co) composites

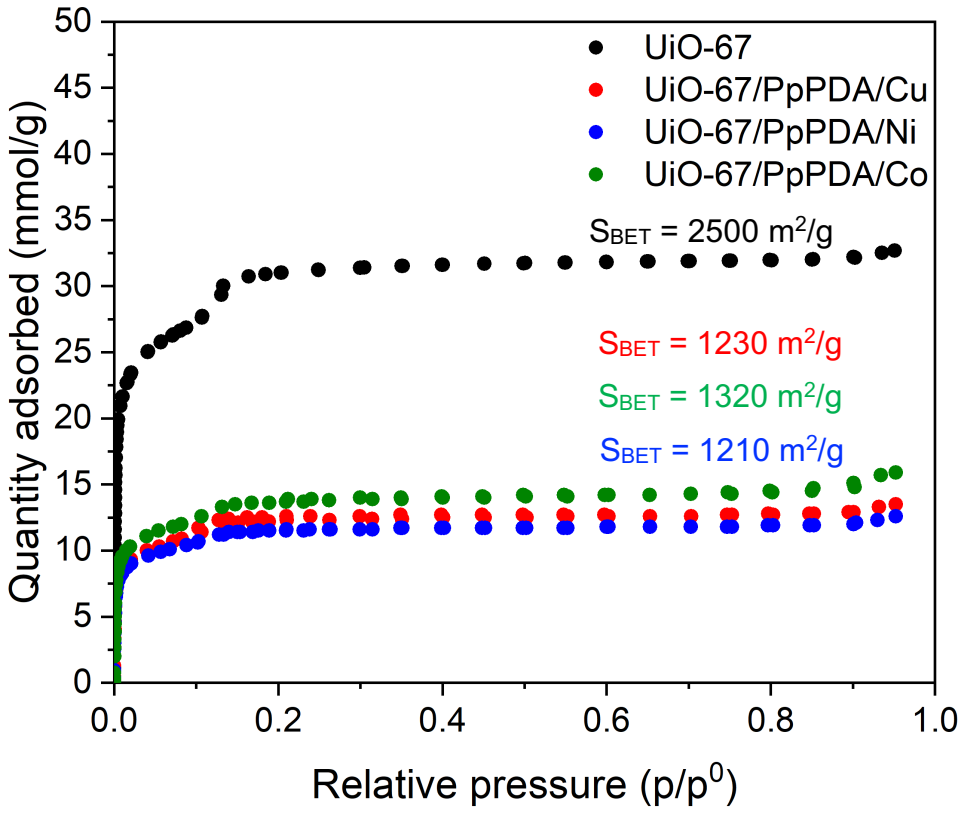

Figure S24 Nitrogen sorption isotherms of the UiO-67/PpPDA/M (M=Cu, Ni and Co) composites

^{1}H NMR characterization for all products

Figure S25:

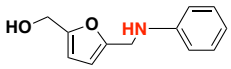

(5-((phenylamino)methyl)furan-2-yl)methanol

Pale yellow oil, 46 mg, 94.5 % yield.

^{1}H NMR ($CDCl_3$, 400MHz, TMS) δ 4.31 (s, 2H, CH_2NH), 4.58 (s, 2H, CH_2OH), 6.18 (d, J = 3.0 Hz, 1H, furan H), 6.22 (d, J = 3.0 Hz, 1H, furan H), 6.64-6.76 (m, 3H, aromatic H), 7.16-7.21 (m, 2H, aromatic H)

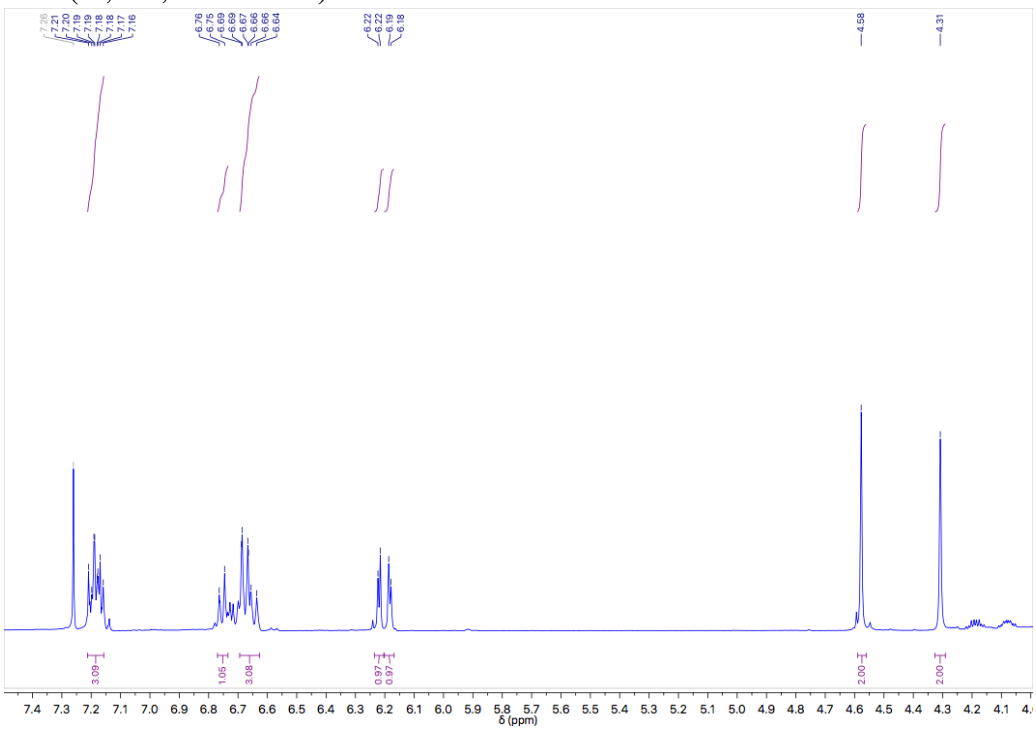

Figure S25 ^{1}H NMR for (5-((phenylamino)methyl)furan-2-yl)methanol

Figure S26:

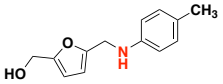

(5-(((4-methylphenyl)amino)methyl)furan-2-yl)methanol
Colourless oil, 47.39 mg, 91 % yield
^{1}H NMR ($CDCl_3$, 400MHz, TMS) δ 2.25 (m, 3H, OMe) 4.27 (s, 2H, CH_2NH), 4.55 (s, 2H, CH_2OH), 6.17 (d, J = 3.0 Hz, 1H, furan H), 6.21 (d, J = 3.0 Hz, 1H, furan H), 6.59-6.63 (m, 2H, aromatic H), 6.96-7.01 (m, 2H, aromatic H)

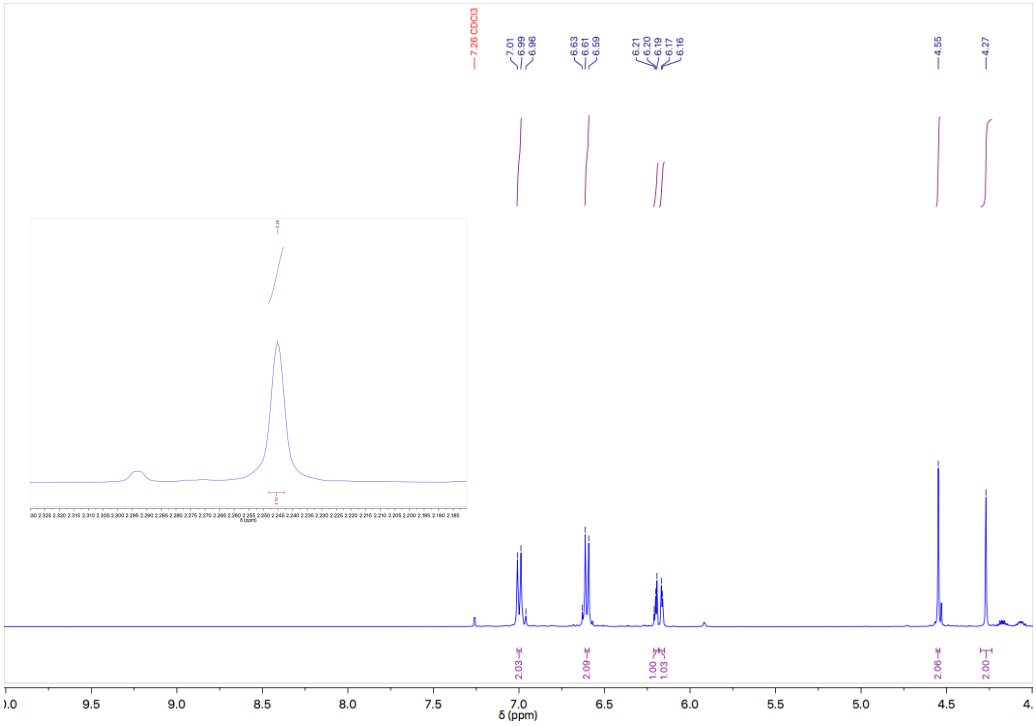

Figure S26 ^{1}H NMR spectra for (5-(((4-methylphenyl)amino)methyl)furan-2-yl)methanol

Figure S27:

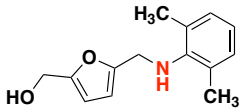

(5-(((2,6-dimethylphenyl)amino)methyl)furan-2-yl)methanol
Colourless oil, 48.23 mg, 87 % yield
^{1}H NMR ($CDCl_3$, 400MHz, TMS) δ 2.19 (m, 6H, OMe) 4.52-4.53 (s, 4H, CH_2NH, CH_2OH), 6.15 (d, J = 3.0 Hz, 1H, furan H), 6.19 (d, J = 3.0 Hz, 1H, furan H), 6.63-6.67 (m, 1H, aromatic H), 6.94-7.02 (m, 2H, aromatic H)

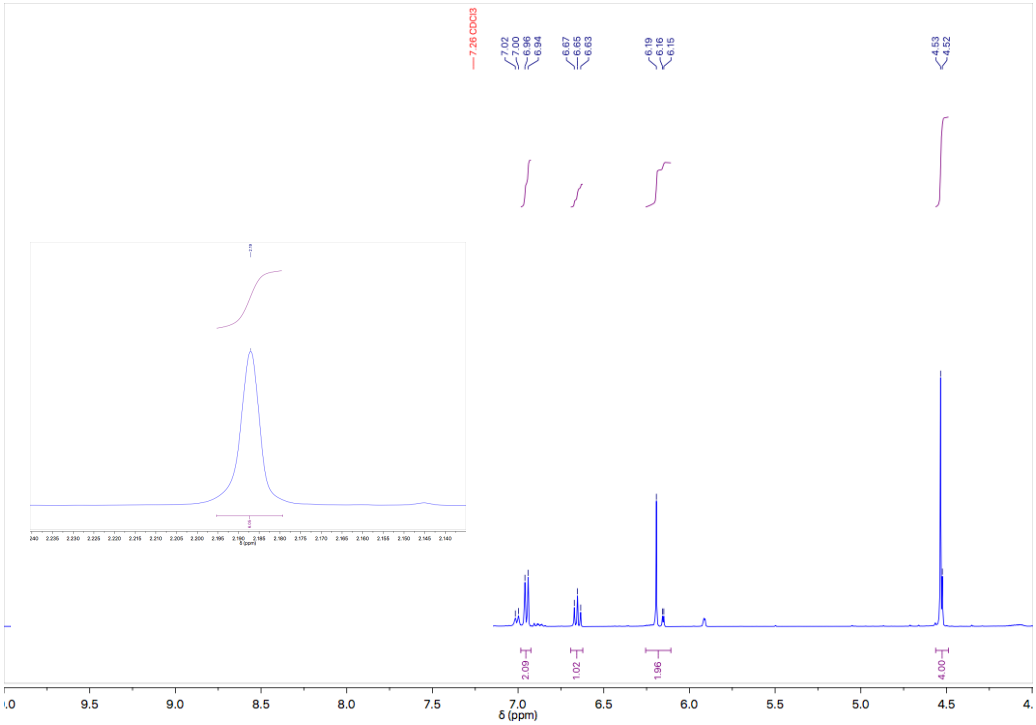

Figure S27 ^{1}H NMR for (5-(((2,6-dimethylphenyl)amino)methyl)furan-2-yl)methanol

Figure S28:

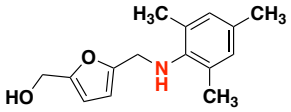

(5-(((2,4,6-trimethylphenyl)amino)methyl)furan-2-yl)methanol
Colourless oil, 40 mg, 68 % yield
^{1}H NMR ($CDCl_3$, 400MHz, TMS) δ 2.16 (m, 9H, OMe) 4.55 (s, 2H, CH_2NH), 4.59 (s, 2H, CH_2OH), 6.16 (d, J = 3.0 Hz, 1H, furan H), 6.24 (d, J = 3.0 Hz, 1H, furan H), 6.77 (s, 6H, OMe, impurity), 6.83-6.85 (m, 2H, aromatic H)

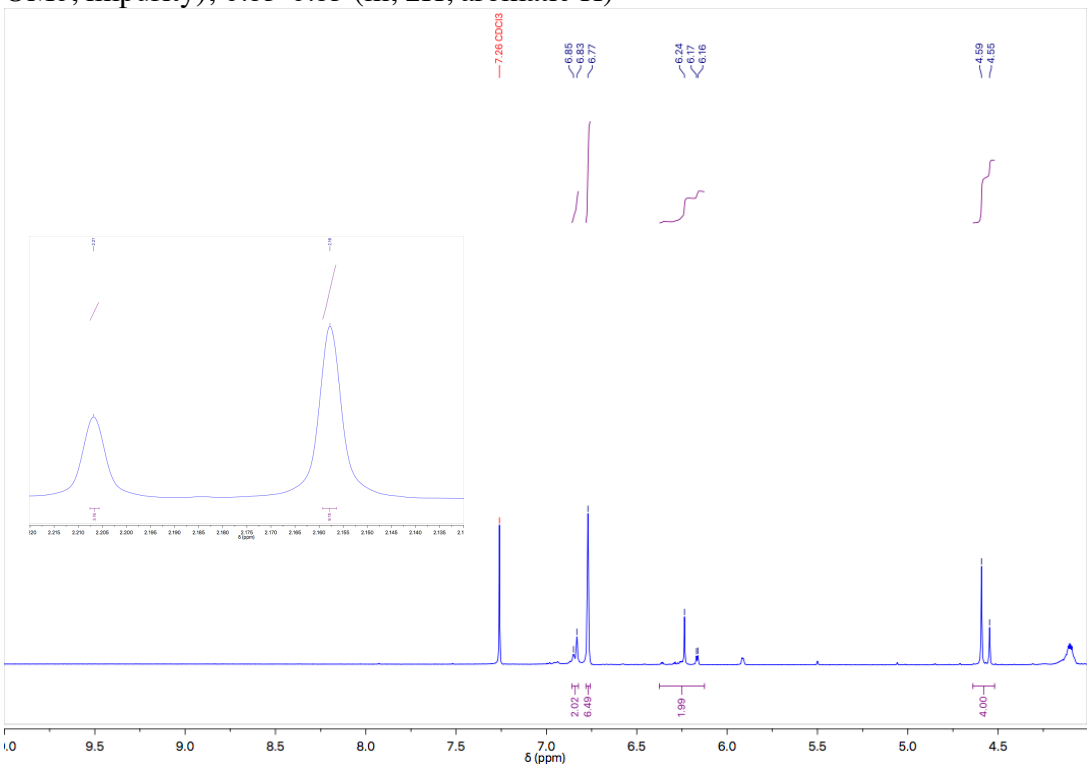

Figure S28 ^{1}H NMR for (5-(((2,4,6-trimethylphenyl)amino)methyl)furan-2-yl)methanol

Figure S29:

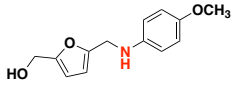

(5-(((4-methoxyphenyl)amino)methyl)furan-2-yl)methanol
Yellow oil, 45 mg, 86 % yield
^{1}H NMR ($CDCl_3$, 400MHz, TMS) δ 3.74 (m, 3H, OMe) 4.24 (s, 2H, CH_2NH), 4.53 (s, 2H, CH_2OH), 6.15 (d, J = 3.0 Hz, 1H, furan H), 6.20 (d, J = 3.0 Hz, 1H, furan H), 6.57-6.64 (m, 2H, aromatic H), 6.75-6.79 (m, 2H, aromatic H)

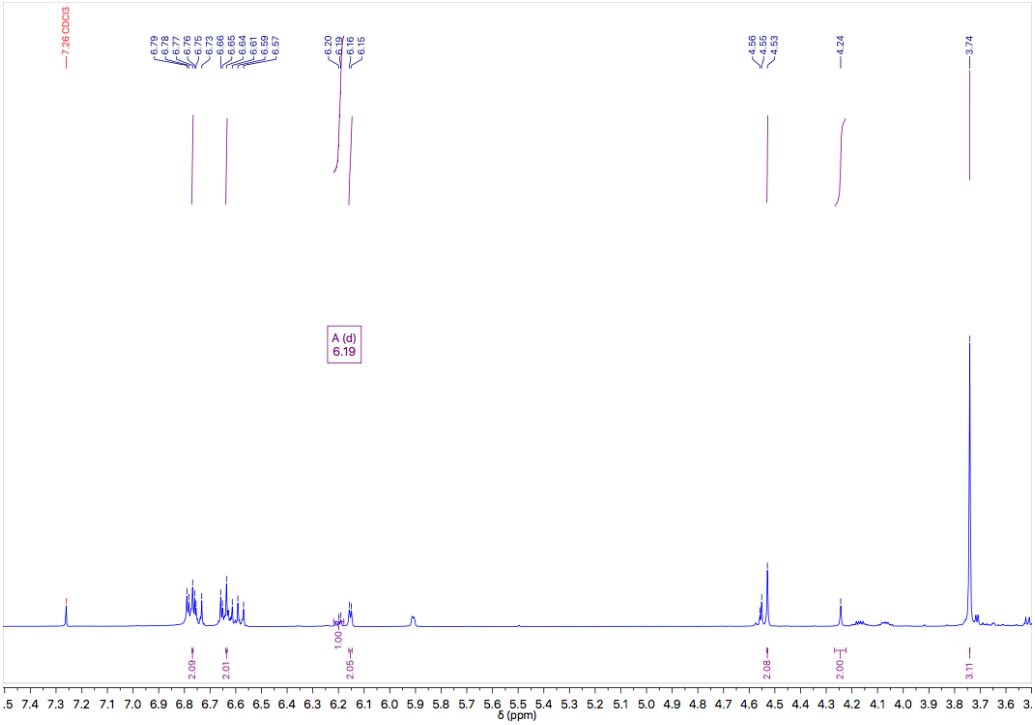

Figure S29 ^{1}H NMR for (5-(((4-methoxyphenyl)amino)methyl)furan-2-yl)methanol

Figure S30:

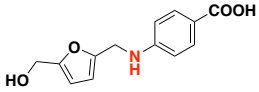

(5-(((4-carboxyphenyl)amino)methyl)furan-2-yl)methanol
Yellow oil, 48 mg, 80 % yield
^{1}H NMR ($CDCl_3$, 400MHz, TMS) δ 4.32 (s, 2H, CH_2NH), 4.55 (s, 2H, CH_2OH), 6.14 (d, J = 3.0 Hz, 1H, furan H), 6.20 (d, J = 3.0 Hz, 1H, furan H), 6.52-6.64 (m, 2H, 2H, aromatic H), 7.90-7.94 (m, 2H, aromatic H)

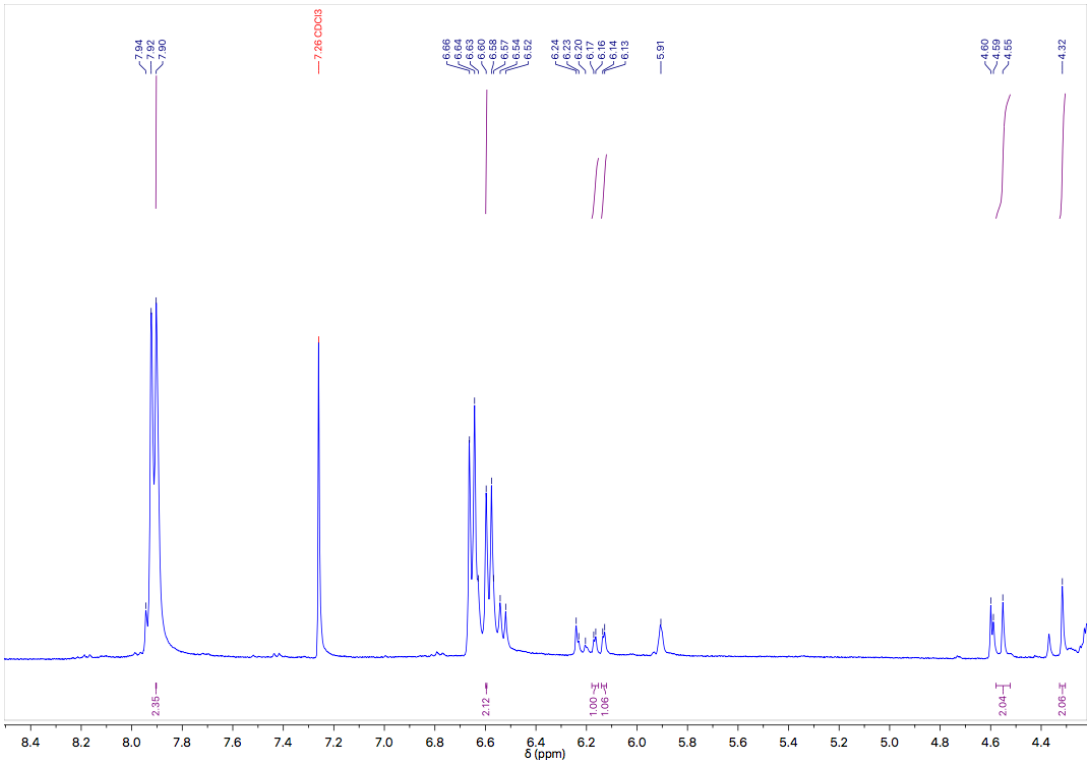

Figure S30 ^{1}H NMR for (5-(((4-carboxyphenyl)amino)methyl)furan-2-yl)methanol

Figure S31:

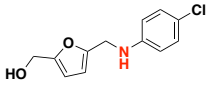

(5-(((4-chlorophenyl)amino)methyl)furan-2-yl)methanol
Colourless oil, 53 mg, 93 % yield
^{1}H NMR ($CDCl_3$, 400MHz, TMS) δ 4.20 (s, 2H, CH_2NH), 4.34 (s, 2H, CH_2OH), 6.17 (d, J = 3.0 Hz, 1H, furan H), 6.20 (d, J = 3.0 Hz, 1H, furan H), 6.64-6.66 (m, 2H, 2H, aromatic H), 7.05-7.09 (m, 2H, aromatic H)

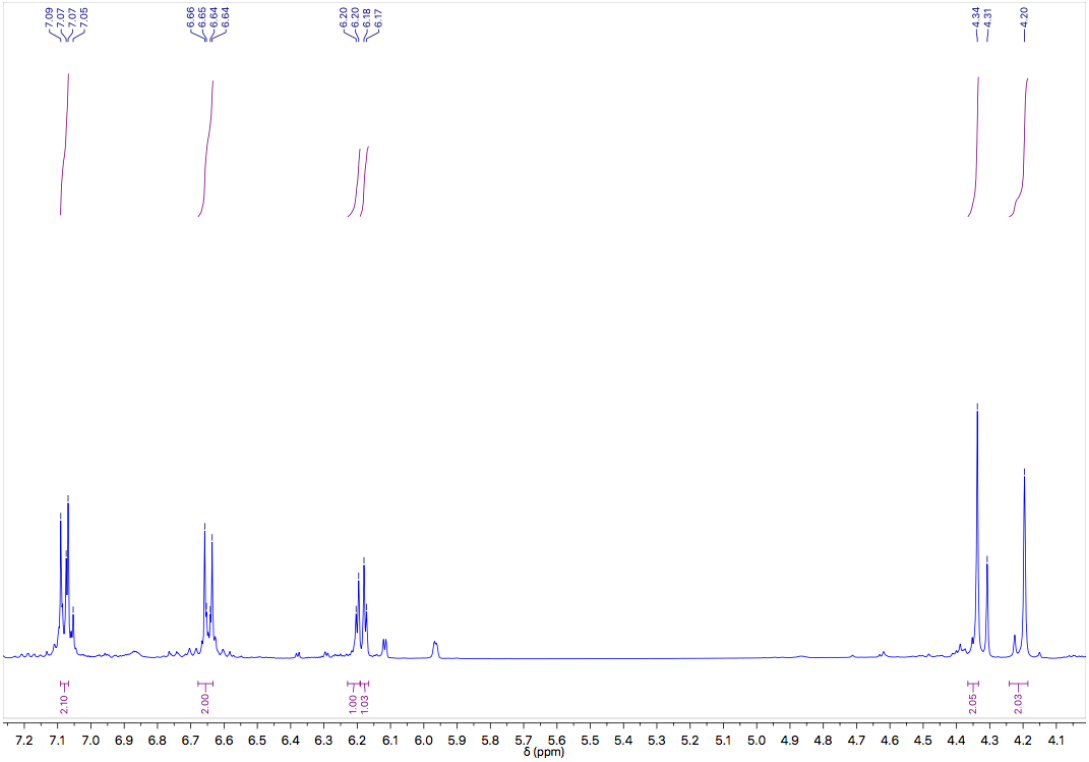

Figure S31 ^{1}H NMR for (5-(((4-chlorophenyl)amino)methyl)furan-2-yl)methanol

Figure S32:

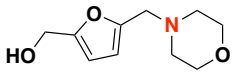

(5-(morpholinomethyl)furan-2-yl)methanol
White solid, 45 mg, 92 % yield
^{1}H NMR ($CDCl_3$, 400MHz, TMS) δ 2.45 (t, J = 4.8 Hz, 4H, CH_2OCH_2) 3.49 (s, 2H, $CH_2N(CH_2CH_2)_2$), 3.70 (t, J = 4.8 Hz, 4H, $CH_2N(CH_2CH_2)_2$), 4.55 (s, 2H, CH_2OH), 6.15 (d, J = 3.0 Hz, 1H, furan H), 6.20 (d, J = 3.0 Hz, 1H, furan H)

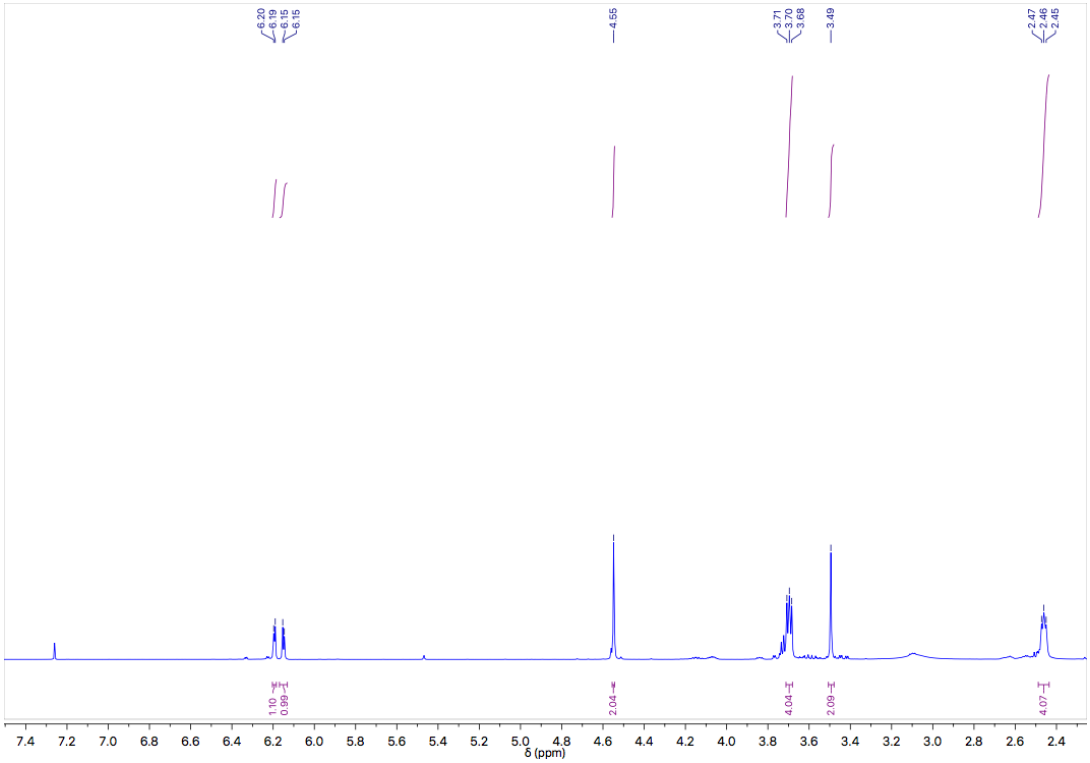

Figure S32 ^{1}H NMR for (5-(morpholinomethyl)furan-2-yl)methanol

Figure S33:

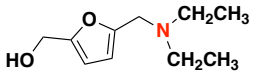

(5-((diethylamino)methyl)furan-2-yl)methanol
Colourless oil, 30 mg, 70 % yield
^{1}H NMR ($CDCl_3$, 400MHz, TMS) δ 1.06 (t, J = 6.8 Hz, 6H, Me) 1.20-1.24 (m, 4H, CH_2CH_2), 3.62 (s, 2H, CH_2N), 4.53 (s, 2H, CH_2OH), 6.15 (d, J = 3.0 Hz, 1H, furan H), 6.20 (d, J = 3.0 Hz, 1H, furan H)

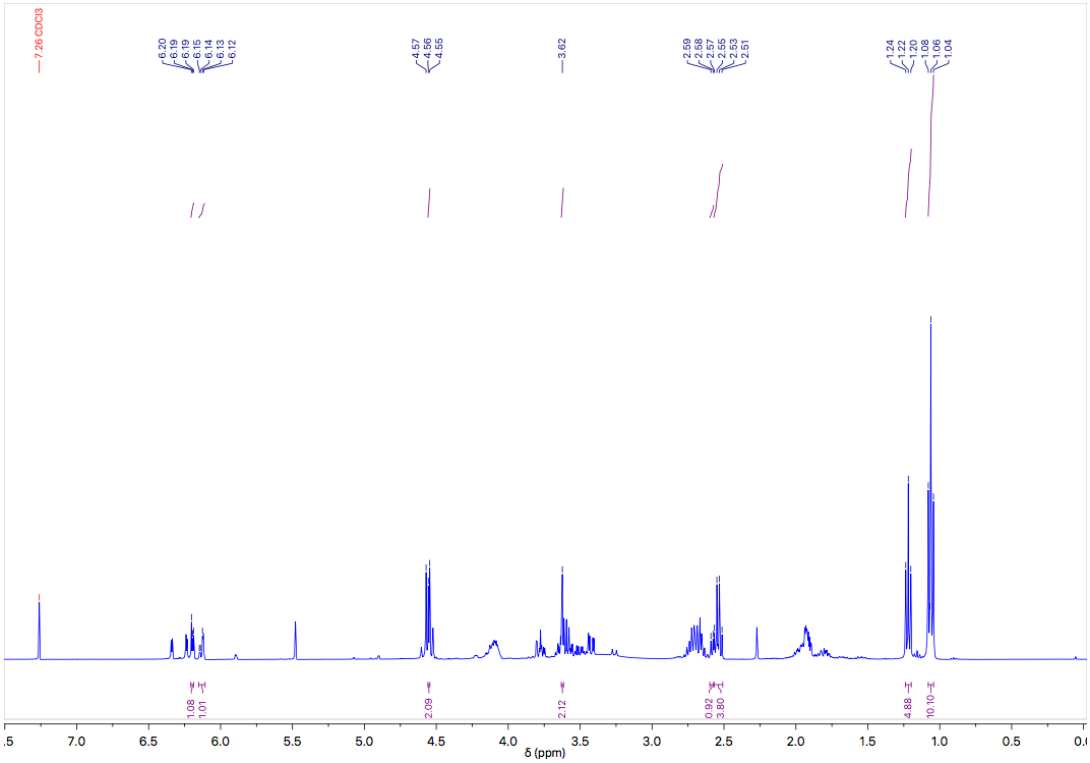

Figure S33 ^{1}H NMR for (5-((diethylamino)methyl)furan-2-yl)methanol

Figure S34:

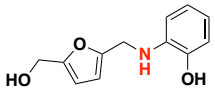

(5-(((2-hydroxyphenyl)amino)methyl)furan-2-yl)methanol
Yellow oil, 44 mg, 83 % yield
^{1}H NMR ($CDCl_3$, 400MHz, TMS) δ 4.25 (s, 2H, CH_2NH), 4.55 (s, 2H, CH_2OH), 6.17 (d, J = 3.0 Hz, 1H, furan H), 6.20 (d, J = 3.0 Hz, 1H, furan H), 6.24 (m, 2H, aromatic H), 6.97-7.03 (m, 2H, aromatic H)

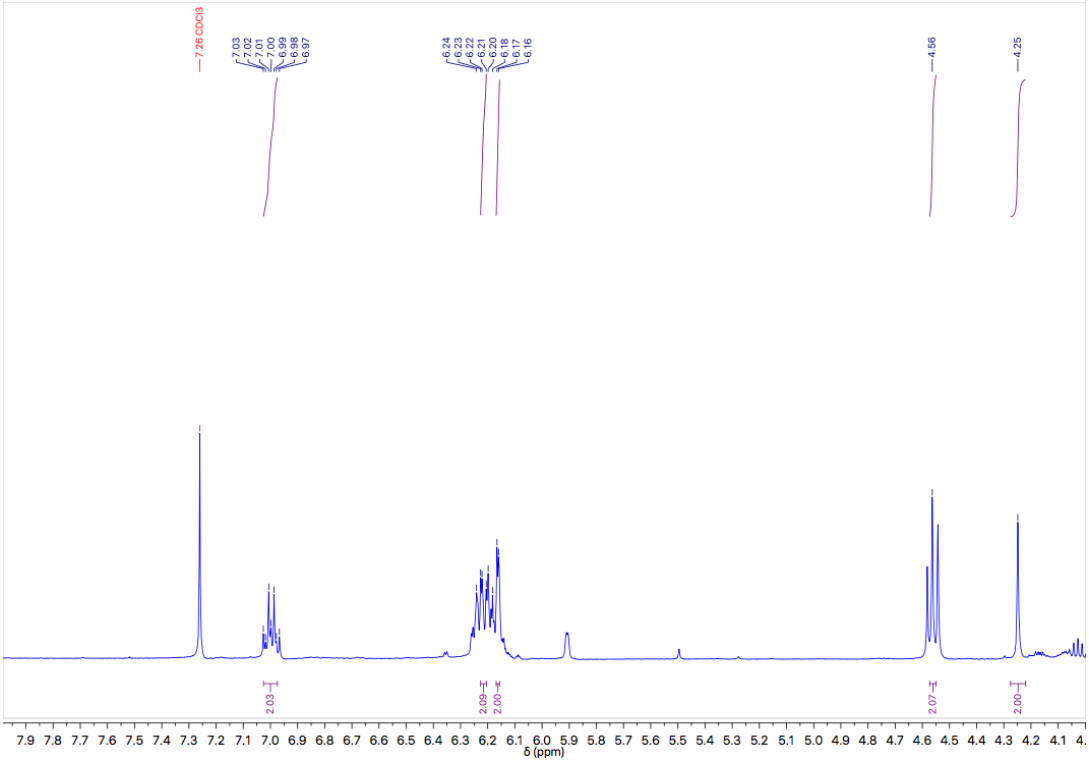

Figure S34 ^{1}H NMR for (5-(((2-hydroxyphenyl)amino)methyl)furan-2-yl)methanol

Figure S35:

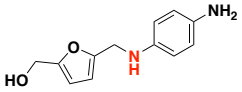

(5-(((4-methoxyphenyl)amino)methyl)furan-2-yl)methanol
Deep red oil, 45 mg, 87 % yield
^{1}H NMR ($CDCl_3$, 400MHz, TMS) δ 4.19 (s, 2H, CH_2NH), 4.50 (s, 2H, CH_2OH), 6.12 (d, J = 3.0 Hz, 1H, furan H), 6.15 (d, J = 3.0 Hz, 1H, furan H), 6.55-6.58 (m, 4H, aromatic H)

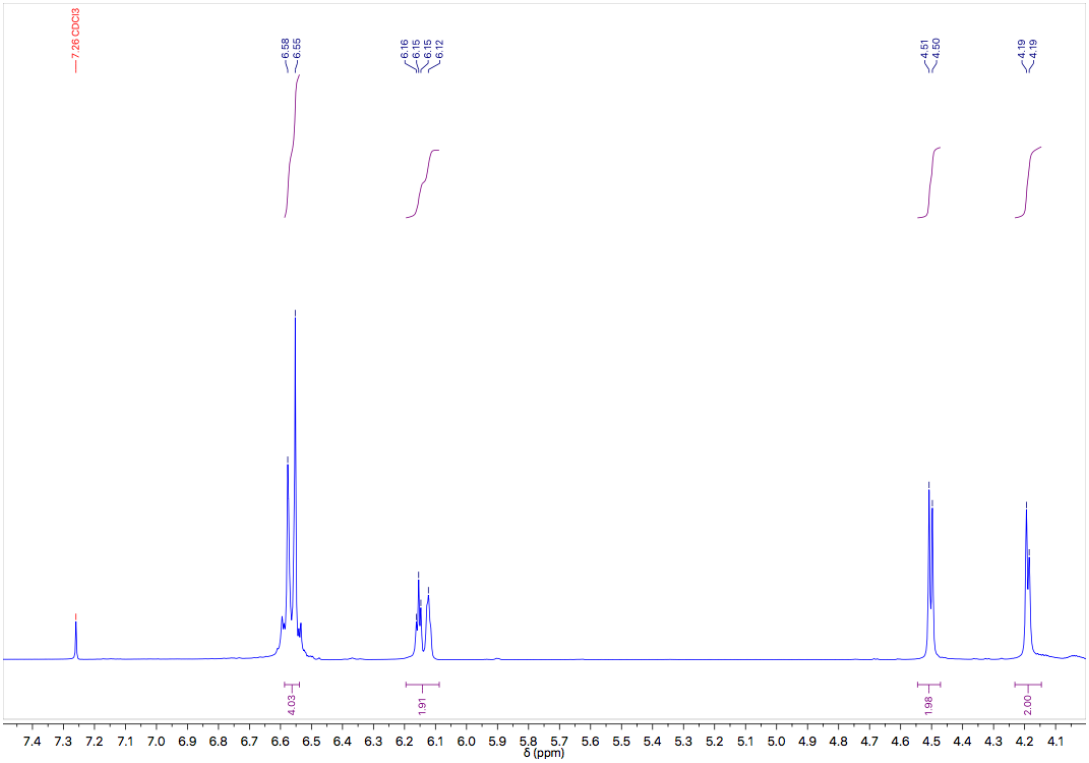

Figure S35 ^{1}H NMR for (5-(((4-methoxyphenyl)amino)methyl)furan-2-yl)methanol

Figure S36:

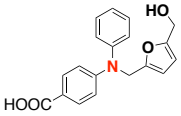

(5-(((4-carboxyphenyl)phenylamino)methyl)furan-2-yl)methanol
White solid, 70 mg, 91 % yield
^{1}H NMR ($CDCl_3$, 400MHz, TMS) δ 4.56 (s, 2H, CH_2N), 4.73 (s, 2H, CH_2OH), 6.29 (d, J = 3.0 Hz, 1H, furan H), 6.55 (d, J = 3.0 Hz, 1H, furan H), 6.74-6.77 (m, 2H, aromatic H), 7.11-7.15 (m, 2H, aromatic H), 7.22-7.24 (m, 3H, aromatic H), 7.33-7.39 (m, 4H, aromatic H), 8.03-8.05 (m, 2H, aromatic H)

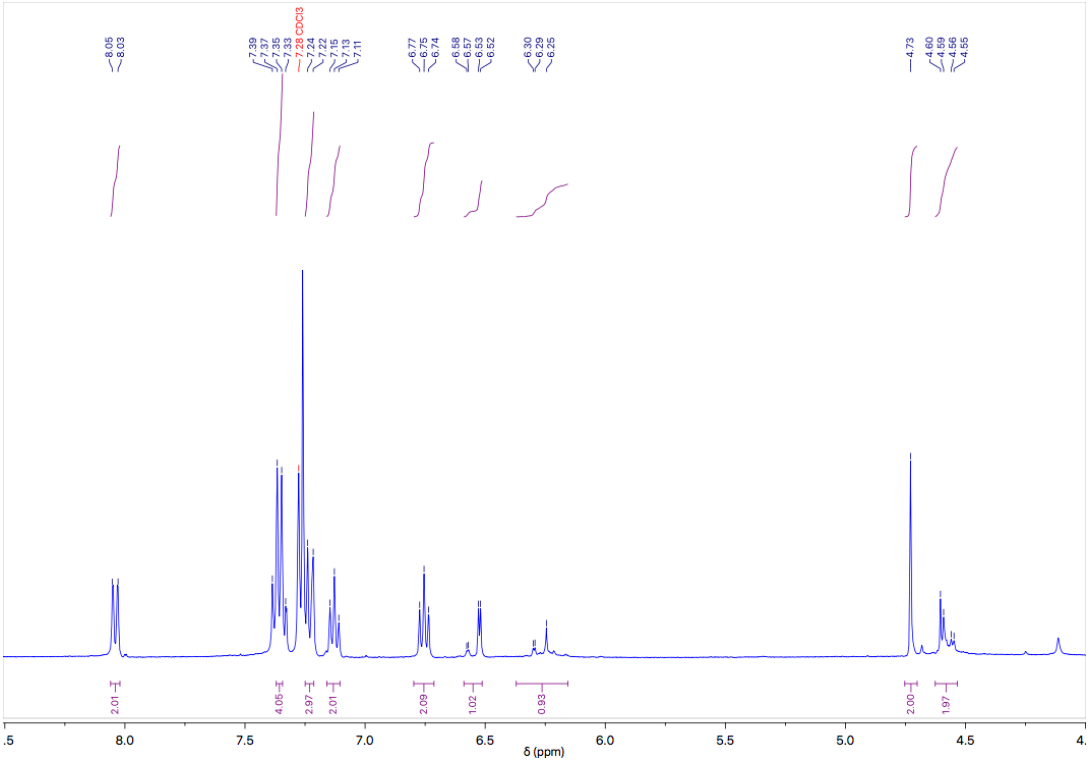

Figure S36 ^{1}H NMR for (5-(((4-carboxyphenyl)phenylamino)methyl)furan-2-yl)methanol

Figure S37 :

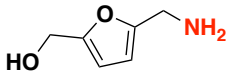

(5-((aminomethyl)furan-2-yl)methanol
Yellow oil, 45 mg, 87 % yield
^{1}H NMR ($CDCl_3$, 400MHz) δ 2.91 (br, 2H, NH_2), 3.75 (s, 2H, CH_2NH_2), 4.54 (s, 2H, CH_2OH), 6.12 (d, J = 3.0 Hz, 1H, furan H), 6.19 (d, J = 3.0 Hz, 1H, furan H)

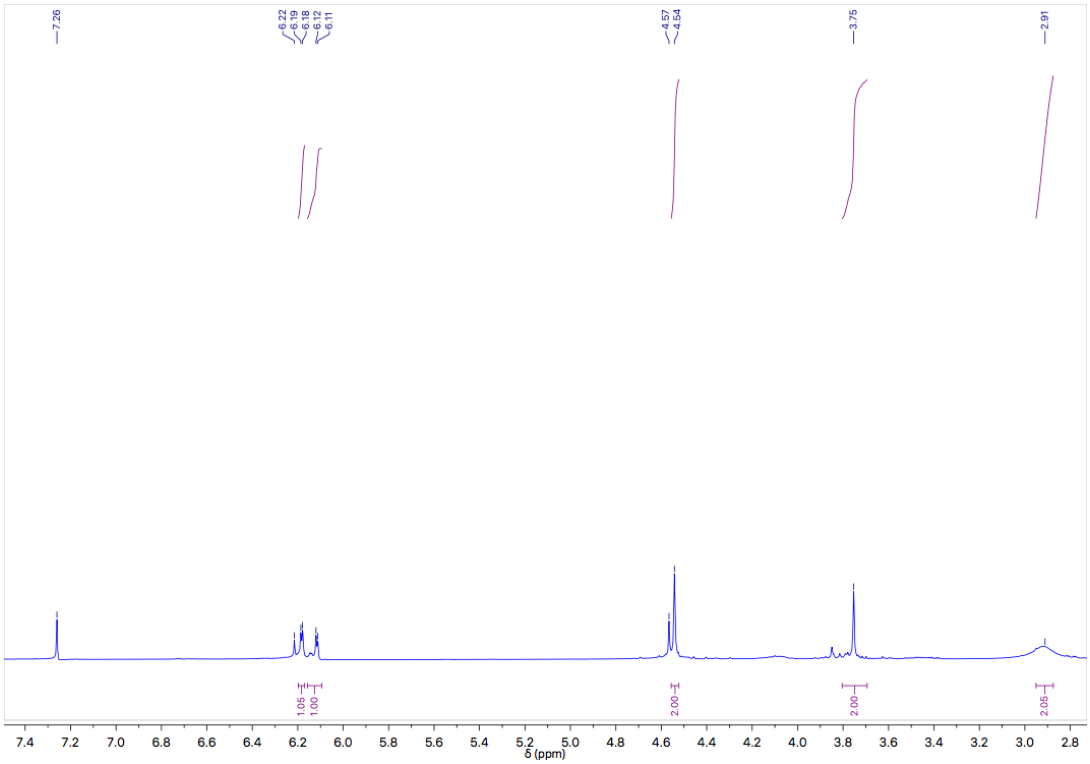

Figure S37 ^{1}H NMR for (5-((aminomethyl)furan-2-yl)methanol

Figure S38:

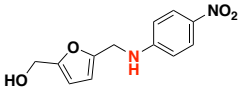

(5-(((4-nitrophenyl)amino)methyl)furan-2-yl)methanol
Red oil, 54 mg, 90 % yield
^{1}H NMR ($CDCl_3$, 400MHz, TMS) δ 4.58 (s, 2H, CH_2NH), 4.78 (s, 2H, CH_2OH), 6.52 (d, J = 3.0 Hz, 1H, furan H), 6.61 (d, J = 3.0 Hz, 1H, furan H),6.64 (m, 1H, aromatic H), 7.21-7.22 (m, 1H, aromatic H), 8.06-8.09 (m, 2H, aromatic H)

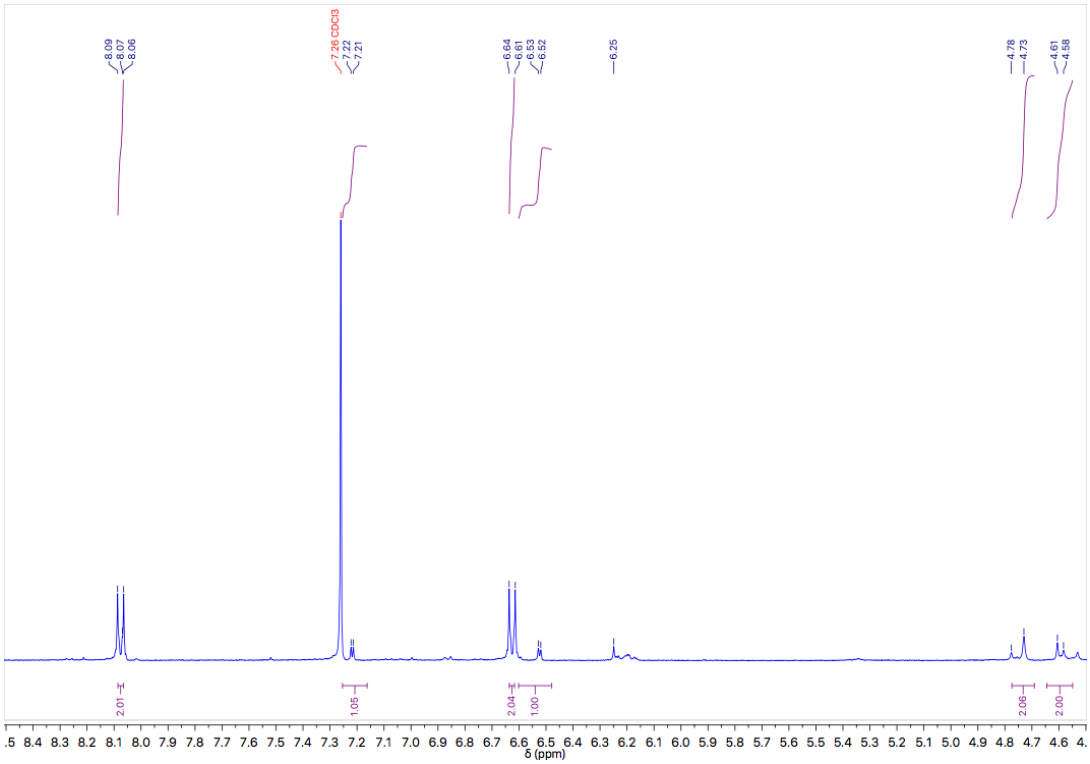

Figure S38 ^{1}H NMR for (5-(((4-nitrophenyl)amino)methyl)furan-2-yl)methanol

Figure S39:

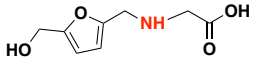

((5-(hydroxymethyl)furan-2-yl)methyl)glycine
Colourless oil, 45 mg, 87 % yield
^{1}H NMR ($CDCl_3$, 400MHz, TMS) δ 3.77 (t, J = 6.9 Hz, 2H, CH_2), 4.19 (s, 2H, CH_2NH), 4.58 (s, 2H, CH_2OH), 6.25 (d, J = 3.0 Hz, 1H, furan H), 6.36 (d, J = 3.0 Hz, 1H, furan H)

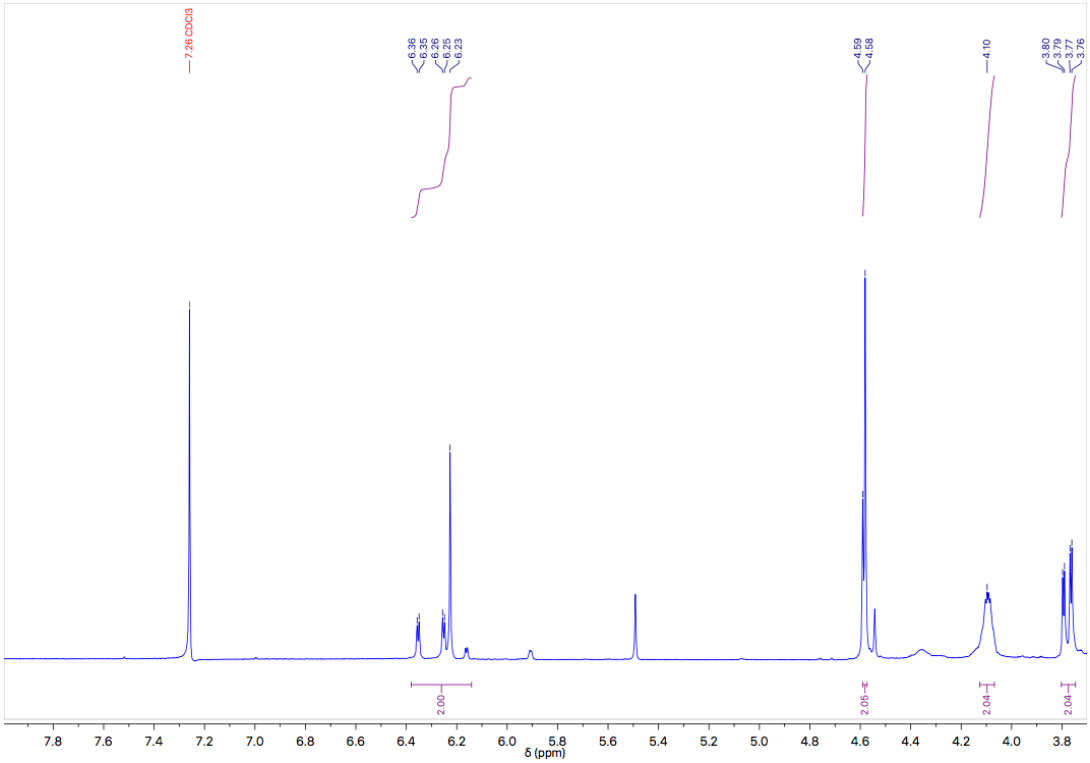

Figure S39 ^{1}H NMR for ((5-(hydroxymethyl)furan-2-yl)methyl)glycine

Figure S40:

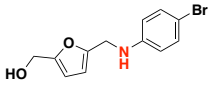

(5-(((4-bromophenyl)amino)methyl)furan-2-yl)methanol
Yellow solid, 65 mg, 96 % yield
^{1}H NMR ($CDCl_3$, 400MHz, TMS) δ 4.31 (s, 2H, CH_2NH), 4.54 (s, 2H, CH_2OH), 6.12 (d, J = 3.0 Hz, 1H, furan H), 6.18 (d, J = 3.0 Hz, 1H, furan H), 7.30-7.33 (m, 4H, aromatic H)

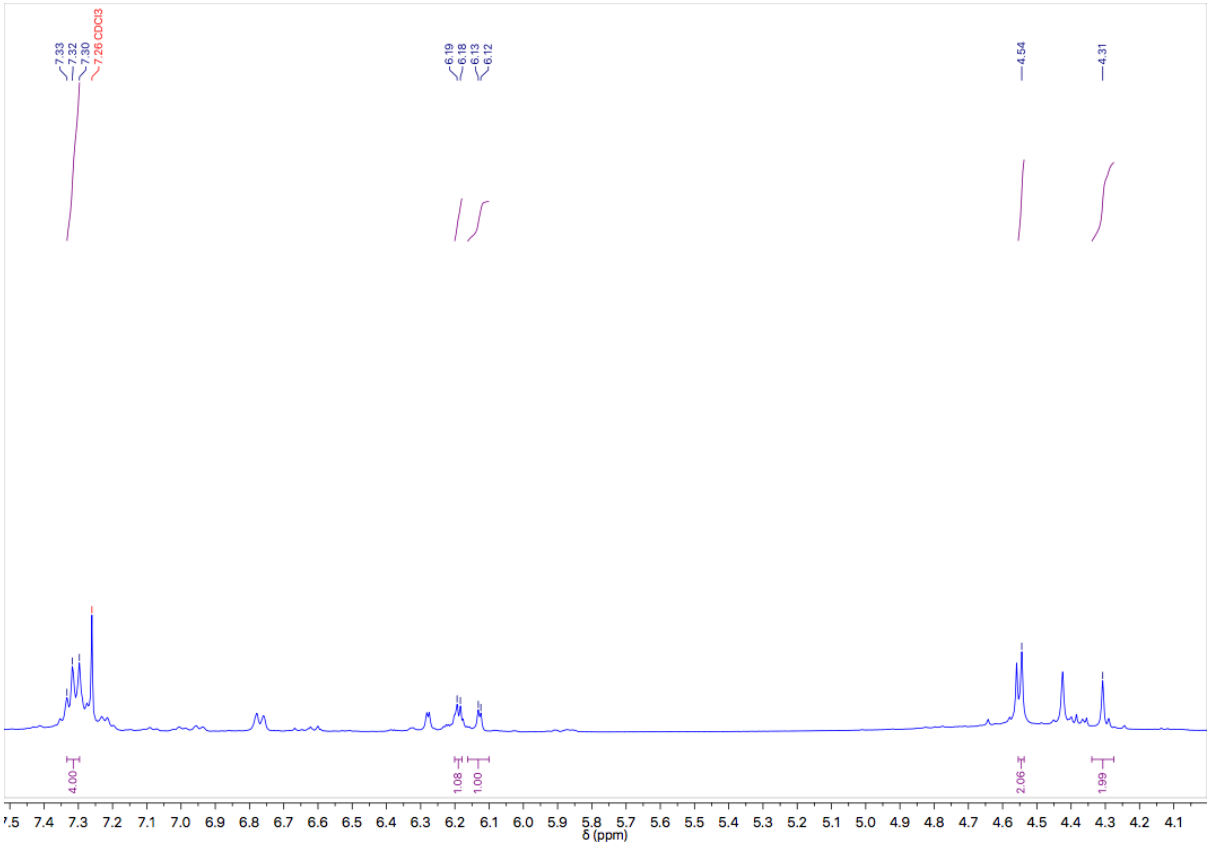

Figure S40 ^{1}H NMR for (5-(((4-bromophenyl)amino)methyl)furan-2-yl)methanol

References:

1. S. Kozuch, J. M. L. Martin, ACS Catalysis, 2012, **2**, 2787-2794.
2. M. Zhu, L. Tao, Q. Zhang, J. Dong, Y. Liu, H. He, Y. Cao, Green Chemistry, 2017, **19**, 3880-3887.
3. R. V. Jagadeesh, K. Murugesan, A. S. Alshammari, H. Neumann, M. Pohl, J. Radnik, M. Beller, Science, 2017, **358**, 326-332.
4. T. Komanoya, T. Kinemura, Y. Kita, K. Kamata, M. Hara, Journal of the American Chemical Society, 2017, **139**, 11493-11499.
5. A. Dunbabin, F. Subrizi, J. M. Ward, T. D. Sheppard, H. C. Hailes, Green Chemistry, 2017, **19**, 397-404.
6. M. Chatterjee, T. Ishikaza, H. Kawanami, Green Chemistry, 2016, **18**, 487-496.
7. T. Matsumura, M. Nakada, Tetrahedron Letters, 2014, **55**, 1829-1834.
8. H. Yang, X. Cui, Y. Deng, F. Shi, Synthetic Communications, 2014, **44**, 1314-1322.
9. M. Mirza-Aghayan, M. Tavana, M. Rahimifard, R. Boukherroub, Applied Organometallic Chemistry, 2014, **28**, 113-115.
10. J. R. Bernardo, S. C. A. Sousa, P. R. Florindo, M. Wolff, B. Machura, A. C. Fernandes, Tetrahedron, 2013, **69(43)**, 9145-9154.
11. V. Kumar, S. Sharma, U. Sharma, B. Singh, N. Kumar, Green Chemistry, 2013, **14**, 3410-3414.
12. D. B. Bagal, R. A. Watile, M. V. Khedkar, K. P. Dhake, B. M. Bhanage, Catalysis Science and Technology, 2012, **2**, 354-358.
13. A. Shokrolahi, A. Zali, M. Keshavarz, Green Chemistry Letter Reviews, 2011, **4(3)**, 195-203.
14. J. Deng, L. Mo, F. Zhao, L. Hou, L. Yang, Z. Zhang, Green Chemistry, 2011, **13**, 2576-2584.
15. R. Lokhande, J. Sonawane, A. Roy, L. Ravishankar, Green Chemistry Letter Reviews, 2011, **4(1)**, 69-72.
16. S. Enthaler, ChemCatChem, 2010, **2**, 1411-1415.
17. S. Enthaler, Catalysis Letters, 2011, **141**, 155-161.
18. R. C. Klet, Y. Liu, T. C. Wang, J. T. Hupp, O. K. Farha, Journal of Material Chemistry A, 2016, **4**, 1479-1485.